

IFJPAN-IV-2015-12

**Study of variants for Monte Carlo generators of  $\tau \rightarrow 3\pi\nu$  decays.****Z. Was and J. Zaremba***Institute of Nuclear Physics, PAN, Kraków, ul. Radzikowskiego 152, Poland***Abstract**

Low energy QCD (below 2 GeV) is a region of resonance dynamics, sometimes lacking satisfactory description as compared to precision of available experimental data. Hadronic  $\tau$  decays offer a probe for such energy regime. In general, predictions for decays are model dependent, with parameters fitted to experimental results. Parameterizations differ by amount of assumptions and theoretical requirements taken into account. Both model distributions and acquired data samples used for fits are results of complex effort.

In this paper, we investigate main parameterizations of  $\tau$  decay matrix elements for the one- and three-prong channels of three-pion  $\tau$  decays. Differences in analytical forms of the currents and resulting distributions used for comparison with the experimental data are studied. We use invariant mass spectra of all possible pion pairs and the whole three-pion system. Also three-dimensional histograms spanned over all distinct squared invariant masses are used to represent results of models and experimental data.

We present distributions from TAUOLA Monte Carlo generation and semi-analytical calculation. These are necessary steps in development for fitting in as model-independent way as possible, and to explore multi-million event experimental data samples. This includes response of distributions to model variants, and/or numerical values of parameters. Interference effects of currents parts are also studied.

For technical purposes, weighted events are introduced. Even though we focus on  $3\pi\nu_\tau$  modes, technical aspects of our study are relevant for all  $\tau$  decay modes into three hadrons.

IFJPAN-IV-2015-12

August 2015

---

<sup>†</sup> This project is financed in part from funds of Polish National Science Centre under decision DEC-2011/03/B/ST2/00107.

# 1 Introduction

One aspect of phenomenological work is to represent theory and experimental efforts in form of Monte Carlo generators. Then, user should be able to obtain any distribution of interest. All details of the detector response can be taken into account if needed. Introduction to the tasks of modeling with the help of Monte Carlo of low energy hadronic interactions can be found, e.g., in [1], and will not be repeated here. We will concentrate on  $\tau$  lepton decays.

Let us point out that there are various aspects of the work for construction of Monte Carlo, which need to be combined. On the theoretical side, assumptions have to be translated into distributions, which can be confronted with the data. This task is easy, if underlying theory is well-established and its calculation methods based, e.g., on perturbation expansions, are converging sufficiently fast. For theorists, it would be ideal if experimental results were represented in a form of background-subtracted and detector corrected distributions, sufficient to constrain all constants (masses, widths, couplings) introduced by the theory (or model) used as a basis for the calculation.

In practice, such a task is often far from being straightforward. Assumptions behind theoretical calculations are often not well-established and the number of phenomenological constants introduced may be too large to be constrained by experimental data.

From the point of view of Monte Carlo techniques, generating processes such as  $\tau$  decays into  $3\pi\nu$  is rather simple. However, necessary for that purpose, hadronic currents span distributions over eight-dimensional space and are the result of a massive effort. Taking into account Lorentz invariance and properties of weak couplings of  $\tau$ -lepton to intermediate virtual  $W$  boson, predictions still require *four* complex scalar functions  $F_i$  of *three* variables each (see the definition later in the text). Such parameterization of matrix elements is commonly used by  $\tau$  decays Monte Carlo generators, e.g., by TAUOLA; and since its beginning [2, 3].

In principle, all properties of the matrix element can be constrained from experimental data. All  $F_i$  can be fitted in a model independent way as proposed in [4]. In practice, this is highly non-trivial. Even if necessary for that purpose, direction of  $\tau$  neutrino can be reconstructed, one has to measure from the data at least **7** distributions over three dimensions with sufficient detail. So far, this was never achieved without partial integration over some of the phase-space dimensions. This practical aspect of the phenomenology work should be separated from the previous two (theoretical and experimental ones), and at the same time offer comfortable and flexible usage.

In this paper, we investigate differences and physics motivations for the presently used in TAUOLA hadronic currents of the  $\tau \rightarrow 3\pi\nu_\tau$  decay channels. Let us recall from Ref. [5] comparisons of different parameterizations for case of the decay mode  $\tau \rightarrow 2\pi\nu_\tau$ . In that case, all results are encapsulated in a single one-dimensional distribution. Our analysis, as we will see, must rely at least on three-dimensional distribution. We compare its efficiency to constrain model parameters first with the method when one-dimensional histograms are used only. To evaluate full size of the model differences, integral of  $|wt - 1| = \left| \frac{|M_{model}|^2}{|M_{model'}|^2} - 1 \right|$  over event samples will be used.  $M_{model}$ ,  $M_{model'}$  denote matrix elements for the two

compared model variants. For completeness, we study the case when only total width of the channel is used to constrain the model.

Theoretical principles embedded in the models and remaining freedom for introducing new couplings and/or intermediate resonances has to be studied at the same time. We have to keep in mind that additional contributions to the currents can modify shapes of the distributions in an nonphysical/uncontrolled way and in unexpected regions of the phase-space. This is especially important when dimensionality of experimental distributions is smaller than that of the decay phase-space.

The paper is organized as follows. In Section 2, we present the list of currents used for evaluation of distributions. Detailed description is delegated to Sections 3, 4, 5, and 6; analytic forms of the currents are given. In Section 7, we present basic features and motivations behind models used in data fitting. Section 8 consists of introduction to numerical comparisons and commonly used representations of experimental data employed in fits. Section 9 is devoted to models used by the CLEO collaboration. In the subsections, numerical results and comparisons are presented. Section 10 describes further variants of currents that were never used outside the experimental collaboration but their existence is mentioned in Ref. [6]. Two main CLEO models are then compared with the BaBar model in Section 11. Section 12 provides comparisons between default TAUOLA model and two models based on the Resonance Chiral Lagrangian (RChL) [7]. For this task, we use mainly one-dimensional histograms; results of measurements in such a form are available not only from the CLEO but from the BaBar as well. Such distributions were used to constrain model parameters in many of our studies. Only CLEO used the three-dimensional distributions as an input for fits.

In Section 13 contributions from different parts of currents and their interferences are investigated. We discuss possible consequences of using model assumptions and limited data samples in Section 14. Summary, Section 15, closes the paper. In Appendix A we present arrangements for semi-analytical calculations which can be used for fits into three-dimensional histograms. In Appendix B numerical comparison of results from different models which are of smaller importance are given. Lengthy histograms of three-dimensional form, are given in Appendix C.

## 2 List of currents

In TAUOLA Monte Carlo generator [8, 9] multiple versions of hadronic currents for the two channels of  $\tau \rightarrow 3\pi\nu_\tau$  decay are available. They are the result of theorists effort but also of extensive work of the experimental collaborations. Over time, currents became available for use outside of the experiments. Unfortunately, sometimes these currents are poorly documented. We plan to explicitly present differences in formulae and values of numerical constants for the main currents available for TAUOLA. For others, we will skip some details as they are of lesser importance or are documented in quoted publications.

The following variants of the currents will be discussed:

1. **CLEO publ.** - current described in ref. [6]. This parameterization was developed

for data of the  $\tau \rightarrow \pi^0\pi^0\pi^-\nu_\tau$  decays. Details will be discussed in Sections 4 and 9.

2. **TAUOLA CLEO** - current implemented in TAUOLA. Code of this current was obtained from the CLEO collaboration and distributed with TAUOLA (all its versions since Ref. [8]). See Sections 4 and 9 for details.
3. **TAUOLA CLEO isospin intricate** - this is a variant where isospin rotation from the  $\pi^0\pi^0\pi^-$  to the  $\pi^-\pi^-\pi^+$  channel was performed for intermediate resonances. Numerical constants remained unmodified. Code was obtained from the CLEO collaboration and distributed with TAUOLA (all versions since [8]) but it was never active<sup>1</sup>. See Sections 4 and 9 for details.
4. **TAUOLA BaBar** - parameterization numerically equivalent to the one used in the BaBar collaboration for basic simulations. Details are given in Sections 5 and 11.
5. **TAUOLA RChL 2012** - version of RChL model introduced in TAUOLA in 2012. This model was based on theoretical consideration of that time and fits to invariant mass distributions of  $\pi^-\pi^-\pi^+$  and  $\pi^-\pi^+$  systems [13]. For details see Sections 6 and 12.
6. **TAUOLA RChL** - this is the model motivated by further theoretical consideration, and comparison with experimental data also for  $\pi^-\pi^-$  invariant mass, Ref. [14].
7. **TAUOLA CPC** - outdated parameterization of Monte Carlo generator. Foundation of many technical benchmarks for phase-space and other verifications which are documented in [3]. Also, test distributions documented in Ref. [4] are available.
8. **Pythia CLEO** - the parameterization of Ref. [6] as implemented in Pythia [15]. Current nearly identical to the **TAUOLA CLEO isospin intricate** is used. Currents of Pythia differ only by numerical constants. In the present paper, we use numerical results of Pythia version 8.201. This current will be discussed in Appendix B

At present, **TAUOLA CLEO** is the default choice which should give the same result regardless of which version of TAUOLA is used. It remained unmodified for at least 14 years. It is identical for FORTRAN and C++ implementations. Differences in distributions between **CLEO publ.**, **TAUOLA CLEO**, **TAUOLA CLEO isospin intricate** and **Pythia CLEO** are presented with all technical and numerical aspects. For completeness, we present numerical results from **TAUOLA RChL**. This last current is aimed to represent data with good precision, and at the same time improve relation with present day theoretical calculations. Numerical results for other variants of the currents are given in less detail or are not presented at all.

---

<sup>1</sup> This parameterization is missing validation with experimental publication; only conference contributions [10, 11] announce its existence, while PhD thesis [12] fully describes even more elaborated variant.

### 3 Common mathematical functions

All currents parameterizations use the same basic formulae. Equation (1) defines<sup>2</sup> hadronic current. It is common for all three-scalars decay channels of TAUOLA and with its help matrix element of  $\tau$  decays can be calculated in a straightforward manner [2, 3],

$$\begin{aligned} J^\mu = N & \left\{ T_\nu^\mu [c_1(p_2 - p_3)^\nu F_1 + c_2(p_3 - p_1)^\nu F_2 + c_3(p_1 - p_2)^\nu F_3] \right. \\ & \left. + c_4 q^\mu F_4 - \frac{i}{4\pi^2 F^2} c_5 \epsilon_{\nu\rho\sigma}^\mu p_1^\nu p_2^\rho p_3^\sigma F_5 \right\}, \end{aligned} \quad (1)$$

where  $T_{\mu\nu} = g_{\mu\nu} - Q_\mu Q_\nu / Q^2$  denotes the transverse projector, and  $Q^\mu = (p_1 + p_2 + p_3)^\mu$  is the momentum of the hadronic system<sup>3</sup>. The decay products are ordered  $\pi^- \pi^- \pi^+$  for the three-prong channel and  $\pi^0 \pi^0 \pi^-$  for the one-prong channel and the pions four-momenta<sup>4</sup> are denoted as  $p_1$ ,  $p_2$  and  $p_3$ , respectively. The same ordering is used in further equations also for masses ( $m_i$ ). The  $\epsilon_{\nu\rho\sigma}^\mu$  is the Levi-Civita symbol<sup>5</sup>. In equations of this and the following sections we use notation:  $s_i = (p_j + p_k)^2$  where  $i \neq j \neq k \neq i$ . Constants:  $c_1$ ,  $c_2$ , etc. are Clebsch-Gordan coefficients, defined specifically for particular hadronic current used.

Eqs. (2), (3) and (4) describe Breit-Wigner functions that are later used in definition of form factors:

$$P(S, m_1, m_2) = \frac{\sqrt{(S - (m_1 + m_2)^2)(S - (m_1 - m_2)^2)}}{\sqrt{S}}, \quad (2)$$

$$\Gamma_{L-wave}(S, M, \Gamma, m_1, m_2, L) = \Gamma \frac{M}{\sqrt{S}} \left( \frac{P(S, m_1, m_2)}{P(M^2, m_1, m_2)} \right)^{2L+1}, \quad (3)$$

$$BW(S, M, \Gamma, m_1, m_2, L) = \frac{M^2}{S - M^2 - iM\Gamma_{L-wave}(S, M, \Gamma, m_1, m_2, L)}. \quad (4)$$

These are typical building blocks useful for hadronic currents parameterizations, such as of Gounaris-Sakurai parametrization [16] for  $\rho \rightarrow \pi\pi$ .

### 4 Hadronic current in models of the CLEO category

Let us describe the default, hadronic currents of the CLEO modeling - **TAUOLA CLEO**. In eq. (5), (6) the analytic form of the hadronic current for the  $\tau \rightarrow 2\pi^0 \pi^- \nu_\tau$  decay channel is presented<sup>6</sup>. Its functional form is extracted from TAUOLA code<sup>7</sup> but has a form exactly

<sup>2</sup>We use five form factors instead of four imposed by Lorenz invariance for practical purpose. In principle  $F_3$  can be represented as linear combination of contributions to  $F_1$  and  $F_2$ .

<sup>3</sup>In TAUOLA code defined as PAA(4).

<sup>4</sup>In TAUOLA code represented as PIM1(4), PIM2(4), PIM3(4).

<sup>5</sup>The  $\epsilon_{\nu\rho\sigma}^\mu p_1^\nu p_2^\rho p_3^\sigma$  is coded in subroutine PROD5.

<sup>6</sup>Constants:  $\beta$ ,  $\beta_1$ ,  $\beta_2$  etc. are coded in TAUOLA as BET, BT1, BT2, etc.

<sup>7</sup>Such approach checks if over the years any modifications were (intentionally or not) introduced.

as described in appendix A of Ref. [6]. Notations differ slightly. This form of hadronic current is also used for the  $\tau \rightarrow 2\pi^-\pi^+\nu_\tau$  decay channel in default TAUOLA setup. It will be discussed later why such a choice is justified. In PDG tables Ref. [17], some mesons have the same name but different mass. In our paper;  $a_1(1260)$ ,  $\sigma$  (or  $f_0(500)$ ),  $f_2(1270)$ ,  $f_0(1370)$ ,  $\rho(770)$ ,  $\rho'(1450)$ ,  $K^*(892)$  are used. Finally, meson  $a'_1(1700)$  as in Ref. [6]. Masses in names will be skipped from this point on.

$$\begin{aligned}
F_1 = & \left( \frac{M_{a_1}^2}{Q^2 - M_{a_1}^2 - \frac{iM_{a_1}\Gamma_{a_1}}{1.3281 \cdot 0.806} \cdot WGA(Q^2)} + \beta \frac{M_{a'_1}^2}{Q^2 - M_{a'_1}^2 - \frac{iM_{a'_1}\Gamma_{a'_1}}{1.3281 \cdot 0.806} \cdot WGA(Q^2)} \right) \cdot \\
& \left( \beta_1 \cdot BW(s_1, M_\rho, \Gamma_\rho, m_2, m_3, 1) + \beta_2 \cdot BW(s_1, M_{\rho'}, \Gamma_{\rho'}, m_2, m_3, 1) \right. \\
& - \beta_3 \cdot \frac{(s_3 - m_3^2) - (s_1 - m_1^2)}{3} \cdot BW(s_2, M_\rho, \Gamma_\rho, m_3, m_1, 1) \\
& - \beta_4 \cdot \frac{(s_3 - m_3^2) - (s_1 - m_1^2)}{3} \cdot BW(s_2, M_{\rho'}, \Gamma_{\rho'}, m_3, m_1, 1) \\
& + \beta_5 \cdot \frac{(Q^2 + s_3 - m_2^2)(2m_3^2 + 2m_1^2 - s_3)}{18s_3} \cdot BW(s_3, M_{f_2}, \Gamma_{f_2}, m_1, m_2, 2) \\
& + \beta_6 \cdot \frac{2}{3} \cdot BW(s_3, M_\sigma, \Gamma_\sigma, m_1, m_2, 0) \\
& \left. + \beta_7 \cdot \frac{2}{3} \cdot BW(s_3, M_{f_0}, \Gamma_{f_0}, m_1, m_2, 0) \right), \tag{5}
\end{aligned}$$

$F_2$  has the same functional form as  $F_1$ . The only difference is interchange for its arguments indices 1 and 2 in eq. (1), and that constant  $c_2$  has opposite sign to  $c_1$ . Note, that  $\beta$  is always set to 0. We suspect that it was introduced by the CLEO collaboration for studies of  $a'_1$  influence.

$$\begin{aligned}
F_3 = & \left( \frac{M_{a_1}^2}{Q^2 - M_{a_1}^2 - \frac{iM_{a_1}\Gamma_{a_1}}{1.3281 \cdot 0.806} \cdot WGA(Q^2)} + \beta \frac{M_{a'_1}^2}{Q^2 - M_{a'_1}^2 - \frac{iM_{a'_1}\Gamma_{a'_1}}{1.3281 \cdot 0.806} \cdot WGA(Q^2)} \right) \cdot \\
& \left( \beta_3 \cdot \frac{(s_2 - m_2^2) - (s_3 - m_3^2)}{3} \cdot BW(s_1, M_\rho, \Gamma_\rho, m_2, m_3, 1) \right. \\
& + \beta_3 \cdot \frac{(s_3 - m_3^2) - (s_1 - m_1^2)}{3} \cdot BW(s_2, M_\rho, \Gamma_\rho, m_3, m_1, 1) \\
& + \beta_4 \cdot \frac{(s_2 - m_2^2) - (s_3 - m_3^2)}{3} \cdot BW(s_1, M_{\rho'}, \Gamma_{\rho'}, m_2, m_3, 1) \\
& + \beta_4 \cdot \frac{(s_3 - m_3^2) - (s_1 - m_1^2)}{3} \cdot BW(s_2, M_{\rho'}, \Gamma_{\rho'}, m_3, m_1, 1) \\
& - \beta_5 \cdot \frac{(s_1 - m_1^2) - (s_2 - m_2^2)}{2} \cdot BW(s_3, M_{f_2}, \Gamma_{f_2}, m_1, m_2, 2) \left. \right). \tag{6}
\end{aligned}$$

Form factors  $F_4$  and  $F_5$  are set to zero<sup>8</sup>. Note, that normalization factor used in  $a_1$  and  $a'_1$  width is the same. The  $Q^2$  dependence of the  $a_1$  width in its propagator is given by the formula<sup>9</sup> (7). It was obtained from analysis performed by the CLEO collaboration [6]. Contributions from the three main  $a_1$  decay channels are taken into account. Complicated form is determined by the decay channels: as  $a_1$  virtuality gets larger thresholds are crossed, allowing more decay channels to open, therefore changing the  $Q^2$  dependence of the effective width.  $Q^2$  is given in GeV<sup>2</sup> units. In the equation below:  $C_{3\pi} = 0.2384^2$  and  $C_{K^*} = 4.7621^2 C_{3\pi}$ .

$$\begin{aligned}
WGA(Q^2) = & \\
C_{3\pi} \cdot \begin{cases} 0 & \text{if } Q^2 < 0.1753, \\ 5.809(Q^2 - 0.1753)^3[1 - 3.0098(Q^2 - 0.1753) + 4.5792(Q^2 - 0.1753)^3] & \text{if } 0.1753 < Q^2 < 0.823, \\ -13.914 + 27.679Q^2 - 13.393Q^4 + 3.1924Q^6 - 0.10487Q^8 & \text{if } Q^2 > 0.823, \end{cases} \\
+ C_{3\pi} \cdot \begin{cases} 0 & \text{if } Q^2 < 0.1676, \\ 6.2845(Q^2 - 0.1676)^3[1 - 2.9595(Q^2 - 0.1676) + 4.3355(Q^2 - 0.1676)^3] & \text{if } 0.1676 < Q^2 < 0.823, \\ -15.411 + 32.088Q^2 - 17.666Q^4 + 4.9355Q^6 - 0.37498Q^8 & \text{if } Q^2 > 0.823, \end{cases} \\
+ C_{K^*} \cdot \begin{cases} \frac{\sqrt{(Q^2 - (M_{K^*} + m_K)^2)(Q - (M_{K^*} - m_K)^2)}}{2Q^2} & \text{if } Q^2 > (M_{K^*} + m_K)^2, \\ 0 & \text{if } Q^2 \leq (M_{K^*} + m_K)^2. \end{cases}
\end{aligned} \tag{7}$$

Let us now turn to the case of **TAUOLA CLEO isospin intricate**. It differs from the previous for the  $\pi^-\pi^-\pi^+$  only. Formulae (5) and (6) are still used for  $\pi^0\pi^0\pi^-$ , but they are replaced by (8) and (9) in the three-prong channel. Those are also extracted from the TAUOLA code, but from part which was not available for the general use.

---

<sup>8</sup> Such choice is dictated by absence of scalar (like  $\pi(1300)$ ) and vector (like  $\omega$ ) intermediate states in this model.

<sup>9</sup> Not all numerical values in the formula below are coming from fits. Explicitly coded numerical constants in TAUOLA have clear physical meaning:  $0.1753 = (3m_\pi)^2$ ,  $0.823 = (M_\rho + m_\pi)^2$ ,  $0.1676 = (2m_{\pi^0} + m_\pi)^2$ .

$$\begin{aligned}
F_1 = & \left( \frac{M_{a_1}^2}{Q^2 - M_{a_1}^2 - \frac{iM_{a_1}\Gamma_{a_1}}{1.3281 \cdot 0.806} \cdot WGA(Q^2)} + \beta \frac{M_{a'_1}^2}{Q^2 - M_{a'_1}^2 - \frac{iM_{a'_1}\Gamma_{a'_1}}{1.3281 \cdot 0.806} \cdot WGA(Q^2)} \right) \cdot \\
& \left( \beta_1 \cdot BW(s_1, M_\rho, \Gamma_\rho, m_2, m_3, 1) + \beta_2 \cdot BW(s_1, M_{\rho'}, \Gamma_{\rho'}, m_2, m_3, 1) \right. \\
& - \beta_3 \cdot \frac{(s_3 - m_3^2) - (s_1 - m_1^2)}{3} \cdot BW(s_2, M_\rho, \Gamma_\rho, m_3, m_1, 1) \\
& - \beta_4 \cdot \frac{(s_3 - m_3^2) - (s_1 - m_1^2)}{3} \cdot BW(s_2, M_{\rho'}, \Gamma_{\rho'}, m_3, m_1, 1) \\
& + \beta_5 \cdot \frac{(s_2 - m_2^2) - (s_3 - m_3^2)}{2} \cdot BW(s_1, M_{f_2}, \Gamma_{f_2}, m_2, m_3, 2) \\
& + \beta_5 \cdot \frac{(Q^2 + s_2 - m_2^2)(2m_3^2 + 2m_1^2 - s_2)}{18s_2} \cdot BW(s_2, M_{f_2}, \Gamma_{f_2}, m_3, m_1, 2) \\
& + \beta_6 \cdot \frac{2}{3} \cdot BW(s_2, M_\sigma, \Gamma_\sigma, m_3, m_1, 0) \\
& \left. + \beta_7 \cdot \frac{2}{3} \cdot BW(s_2, M_{f_0}, \Gamma_{f_0}, m_3, m_1, 0) \right). \tag{8}
\end{aligned}$$

Again,  $F_2$  has the same functional form as  $F_1$ . The only difference is interchange of indices 1 and 2 for its arguments in eq. (1), and that constant  $c_2$  has opposite sign to  $c_1$ .

$$\begin{aligned}
F_3 = & \left( \frac{M_{a_1}^2}{Q^2 - M_{a_1}^2 - \frac{iM_{a_1}\Gamma_{a_1}}{1.3281 \cdot 0.806} \cdot WGA(Q^2)} + \beta \frac{M_{a'_1}^2}{Q^2 - M_{a'_1}^2 - \frac{iM_{a'_1}\Gamma_{a'_1}}{1.3281 \cdot 0.806} \cdot WGA(Q^2)} \right) \cdot \\
& \left( \beta_3 \cdot \frac{(s_2 - m_2^2) - (s_3 - m_3^2)}{3} \cdot BW(s_1, M_\rho, \Gamma_\rho, m_2, m_3, 1) \right. \\
& + \beta_3 \cdot \frac{(s_3 - m_3^2) - (s_1 - m_1^2)}{3} \cdot BW(s_2, M_\rho, \Gamma_\rho, m_3, m_1, 1) \\
& + \beta_4 \cdot \frac{(s_2 - m_2^2) - (s_3 - m_3^2)}{3} \cdot BW(s_1, M_{\rho'}, \Gamma_{\rho'}, m_2, m_3, 1) \\
& + \beta_4 \cdot \frac{(s_3 - m_3^2) - (s_1 - m_1^2)}{3} \cdot BW(s_2, M_{\rho'}, \Gamma_{\rho'}, m_3, m_1, 1) \\
& - \beta_5 \cdot \frac{(Q^2 + s_1 - m_1^2)(2m_2^2 + 2m_3^2 - s_1)}{18s_2} \cdot BW(s_1, M_{f_2}, \Gamma_{f_2}, m_2, m_3, 2) \\
& - \beta_5 \cdot \frac{(Q^2 + s_2 - m_2^2)(2m_3^2 + 2m_1^2 - s_2)}{18s_2} \cdot BW(s_2, M_{f_2}, \Gamma_{f_2}, m_3, m_1, 2) \\
& + \beta_6 \cdot \frac{-2}{3} \cdot BW(s_1, M_\sigma, \Gamma_\sigma, m_2, m_3, 0) \\
& + \beta_6 \cdot \frac{2}{3} \cdot BW(s_2, M_\sigma, \Gamma_\sigma, m_3, m_1, 0) \\
& - \beta_7 \cdot \frac{-2}{3} \cdot BW(s_1, M_{f_0}, \Gamma_{f_0}, m_2, m_3, 0) \\
& \left. - \beta_7 \cdot \frac{2}{3} \cdot BW(s_2, M_{f_0}, \Gamma_{f_0}, m_3, m_1, 0) \right). \tag{9}
\end{aligned}$$

One can ask, why the isospin symmetry was imposed taking into account final states (that means distributions only) in the version of the code used as default in TAUOLA for so many years, even though it is not the property of the model used, see eg. Ref. [18]. We will return to this point later at a time of discussing numerical results. Current of eq. (5) and (6) is used in TAUOLA for one-prong and three-prong of the three-pion channels in most of applications<sup>10</sup>. Note, that neither Ref. [11] nor [10] give functional form of  $\tau \rightarrow 2\pi^-\pi^+\nu_\tau$  current, also Ref. [6] presents functional form of hadronic current for  $\tau \rightarrow 2\pi^0\pi^-\nu_\tau$  only. Parameters used in currents, will be presented later.

## 5 Analytic form of hadronic current of TAUOLA BaBar

This model became public recently, it was developed by the experimental collaboration. Mentioned in Section 1, isospin symmetry and limitation of quality of the data was probably behind the choice of form factors used by BaBar as well. They are the same for  $\tau \rightarrow 2\pi^0\pi^-\nu_\tau$  and  $\tau \rightarrow 2\pi^-\pi^+\nu_\tau$ . BaBar model does not include resonances  $f_0$ ,  $f_2$  and  $\sigma$ . Note, that BaBar choice was introduced after the CLEO currents (both variants) were known and available for them. Equations in this section are extracted from TAUOLA code numerically equivalent to the one used by BaBar<sup>11</sup>.

$$F_1 = \frac{M_{a_1}^2}{Q^2 - M_{a_1}^2 - iM_{a_1}\frac{GFUN(Q^2)}{GFUN(M_{a_1}^2)}} \cdot \begin{cases} BW(s_1, M_\rho, \Gamma_\rho, m_2, m_3, 1) + \frac{\beta_1}{1+\beta_1} BW(s_1, M_{\rho'}, \Gamma_{\rho'}, m_2, m_3, 1) & \text{if } s_1 > (m_\pi + m_\pi)^2, \\ \frac{M_\rho^2}{M_\rho^2 - s_1} + \frac{\beta_1}{1+\beta_1} \frac{M_{\rho'}^2}{M_{\rho'}^2 - s_1} & \text{if } s_1 \leq (m_\pi + m_\pi)^2, \end{cases} \quad (10)$$

$F_2(s_2)$  coincide with  $F_1(s_1)$ . It has an opposite sign as well;  $F_3 = 0$ ;  $F_4 = 0$ ;  $F_5 = 0$ .

$$GFUN(x) = \begin{cases} 4.1(x - 9m_{\pi_0}^2)^3[1 - 3.3(x - 9m_{\pi_0}^2)] + 5.8(x - 9m_{\pi_0}^2)^2 & \text{if } x < (M_\rho + m_\pi)^2, \\ x(1.623 + \frac{10.38}{x} - \frac{9.32}{x^2} + \frac{0.65}{x^3}) & \text{if } x \geq (M_\rho + m_\pi)^2. \end{cases} \quad (11)$$

Note, that eqs. (11) and (7) aim at  $a_1$  phase-space dependence, but eq. (11) does so in simpler manner. CLEO model uses more sophisticated polynomial interpolation with inclusion of  $K^*K$  production threshold; above  $a_1$  can decay relatively abundantly into pair of kaons and a pion.

---

<sup>10</sup> Note, that later the BaBar collaboration was using both of these options as alternative to their default parameterization.

<sup>11</sup> The authors would like to acknowledge Swagato Banerjee and Tomasz Przedzinski for cross-validation of our modifications of the  $\tau \rightarrow 3\pi\nu$  hadronic current called TAUOLA BaBar, with the TAUOLA installation in BaBar framework at a statistical level of 100M events. For comparisons standard distributions prepared with MC-TESTER [19] were used.

## 6 Resonance Chiral Lagrangian currents

Our first hadronic current based on the Resonance Chiral Lagrangian scheme - **TAUOLA RChL 2012** was prepared for Ref. [20]. Similarly to parameterization of BaBar, the same form of current was used for one- and three-prong  $\tau$  decay modes into three pions. As an input for fits, only two, one-dimensional histograms of BaBar data were used. Later on, the invariant mass of  $\pi^-\pi^-$  pair became available. It turned out that contributions which, under isospin symmetry, provide different form of the current for one- and three-prong decay modes was useful. We refer to this later parameterization as **TAUOLA RChL**; it is documented in Ref. [14].

We will return to isospin symmetry aspect, when we will discuss sensitivity of different distributions to specific parts of current contributions. This may hint, why isoscalar terms introduced by CLEO many years ago, were actually dropped out in currents, such as **TAUOLA BaBar** and **TAUOLA RChL 2012**.

## 7 Practical aspects of model construction

There are two main paths to be taken in model building. Empirical approach is to prepare something describing the data in the best possible way, without considering how physical process works. Other choice is to start from theoretical principles, obtain distributions and introduce only necessary adaptations at a time of comparison with data. Of course, merging those two approaches is desirable and even essential. There are unquestioned rules like Lorentz invariance which have to be obeyed. All models used in TAUOLA and in our paper, respect such rules.

In particle physics we expect Breit-Wigner distributions to describe shapes of experimental distributions. One should bear in mind that precision of experimental data of today can be very high. Multiple millions of events were collected for individual  $\tau$  decay channels. On the other hand, once inspection of the assumptions behind theoretical models is performed, rather modest estimations for systematic uncertainties of the predictions are obtained [21]. For example, for RChL models, in Ref. [20] Section 7.4 it was argued that on the basis of theoretical arguments alone, the predicted uncertainty can in principle be as high as 30 %. Even behind such a basic principle like isospin symmetry uncertainty at the level of 5-10 % can be expected at least in some cases, see, e.g., Ref. [1] Section 5.11. That is again more than one order of magnitude worse than precision of the experimental data. Comparing to differences in results of Section 9.2 it is about the same order of magnitude.

That is why, comparison of model's results with the data can be an exciting source of inspiration for further model developments, even if attained agreement with the data is not perfect at the beginning. Such development can be particularly promising for the models precisely representing distributions of several  $\tau$  decay channels and/or final states in  $e^+e^- \rightarrow \text{hadrons}$ .

In case of **TAUOLA CLEO**, at start, model of Ref. [22] was used. With time, as a consequence of comparisons with the data, it evolved into form where Breit-Wigner

resonances seen in experimental data were added. Some of the model assumptions, in particular numerical values of the chiral couplings in soft limit were compromised. One should keep in mind that only at very low energies chiral dynamics is expected to determine unambiguously the hadron form factors probed by semileptonic  $\tau$  decays [23, 24, 25].

At present, more elegant approach is taken; the RChL model. It was started from theoretical calculations accounting to expansion in number of colors  $N_c \rightarrow \infty$  [26, 27]. Later, this model required empirical correction by the  $\sigma$  meson introduced in Ref. [14] as an additional Breit-Wigner. Authors are still working out a way to include  $\sigma$  and possibly other isoscalars within RChL scheme using unitarity and analiticity constraints to include this re-scattering effect.

Other interesting approach in modeling was taken, e.g., in Ref. [28]. It describes hadronic current for  $\tau \rightarrow 4\pi\nu_\tau$ . This modeling is in part data driven. As measurements of  $e^+e^-$  annihilation into four pions arrived [29], they could be used to model distribution of invariant mass of the whole  $4\pi$  system<sup>12</sup>. Authors introduced correction into matrix element to reproduce experimental distribution. Then,  $a_1\pi$  dominance as intermediate state was assumed. From that point on, any desired modeling of  $a_1$  could be used. The one of Ref. [30] was chosen as it was applied for  $e^+e^-$  data as well.

Those are only a few of many possible approaches. There is no straightforward way of telling that one is better than other. Actual choice has to be motivated by quality and precision of experimental data. Let us address this point in the next section.

## 8 Data representations and numerical methods

Experimentalists and theoreticians may prefer distinct forms for data representation in model building, comparisons and fits. In this section we will concentrate on methods we use and those that were used for constraining investigated models in the past.

The most simple way to compare models and also to fit the experimental data is to look only at the total width of the channel<sup>13</sup> (we will call it **option 1**). Such approach is used when there is no sufficient data available for a more advanced fit. Even though it is only one number, it can be used as a first test of particular model. Total width is usually well documented by PDG tables, see, e.g., Ref. [17] including careful analysis of experimental statistical and systematical error.

Next approach is to look at one-dimensional distributions. In this case, one should seek the possibility of having experimental data for all possible invariant mass distributions. This is not always possible. Using as an example the  $\pi^-\pi^-\pi^+$  channel, one must be aware that it is easy to have many models that fit perfectly, let's say the  $\pi^-\pi^-\pi^+$  spectra, while having distributions of  $\pi^-\pi^-$  and  $\pi^-\pi^+$  off. We can articulate 3 options of one-dimensional distributions in use for the case of  $\tau \rightarrow 3\pi\nu_\tau$  current input:

---

<sup>12</sup> It was done by relating  $2\pi^+2\pi^-$  and  $\pi^+\pi^-2\pi^0$  systems produced in  $e^+e^-$  annihilation with  $\pi^+2\pi^-\pi^0$  and  $\pi^-3\pi^0$  produced in  $\tau$  decays. For that, isospin symmetry was applied to distributions measured from  $e^+e^-$  annihilation giving prediction on shapes of four-pion system invariant mass spectra in  $\tau$  decays.

<sup>13</sup> Option 1 was used, e.g., in Ref. [31] for  $5\pi$  currents.

- $\pi^-\pi^-\pi^+$  system invariant mass only<sup>14</sup> (**option 2**).
- $\pi^-\pi^-\pi^+$  and  $\pi^-\pi^+$  invariant masses<sup>15</sup> (**option 3**).
- $\pi^-\pi^-\pi^+$ ,  $\pi^-\pi^+$  and  $\pi^-\pi^-$  invariant masses<sup>16</sup> (**option 4**).

In more advanced approach of **Dalitz distributions** (**option 5**) slices in  $Q^2$  were used already in Ref. [6]. This way of data representation is in nature three-dimensional<sup>17</sup>. Models originating from the CLEO collaboration were fitted in that way. To explore the whole structure of the decay channel methods of Ref. [4] have to be introduced (**option 6**). Up to now, no complete analysis was performed with their help. Only Ref. [6] mentions cross-check with such methods.

Let us turn to practical aspects of our paper comparisons for distributions with options listed above. For that purpose we describe re-weighting method. We use it often due to its numerical efficiency and simplicity. When generating events from Monte Carlo generator for different models, statistically independent event samples are produced. But one may ask what is the probability of getting particular event with certain set of momenta depending on the model we use. Having all momenta of particles in an event, one can calculate the amplitude for such specific configuration. Therefore, one can calculate amplitudes for the event using each model and compare. This leads to the possibility of re-weighting events by using one model as reference and instead of generating a new sample with a different model, calculating amplitudes from that other model for existing events. Ratio of new amplitude squared to old one, can be then attributed to the event as its weight. Thanks to weights use, samples are correlated. Statistical error affects the difference for the compared models only. Using this strategy for a different model we may not only get the new distributions with different shape but also its integral, that is the total width of the channel. Method can be applied to minuscule changes of model parameters, which are needed, e.g., for calculation of derivatives.

Re-weighting events can be used to estimate the contribution from parts of the model amplitude as well. The ratio of investigated part of the amplitude squared to a whole amplitude squared provides then the weight. Evaluation of interferences between parts of currents is also possible on the event by event basis. One has to evaluate how far from 1 is the sum of weights coming from all parts.

Let us look into that in more detail. For any integrated distributions bin always represents average weight of events filling it. Once histogram is filled, information from separate events is lost. Because of that, interference observed in any histogram is reduced with respect to its full size. Effect in integrated distribution is dependent on selection of bins. By comparing interference coming from the event by event analysis and integrated distri-

---

<sup>14</sup> Similar to **option 2** fit was performed for  $4\pi$  current in Ref. [28] with only invariant mass of four pions used.

<sup>15</sup> **Option 3** was used in fits of **TAUOLA RChL 2012**. Probably also BaBar model was fitted in this way.

<sup>16</sup> **Option 4** was used for fits of **TAUOLA RChL**.

<sup>17</sup> There are 8 plots, each in different range of  $Q^2$ ; on x-axis there is  $s_1$  and  $s_2$  is on y-axis.  $s_1$  is always chosen as the bigger of the two possible  $\pi^-\pi^+$  pair invariant masses. See plots of appendix C.

butions one may evaluate how viable used distributions are to constrain interference and if model can be explored with available data sufficiently well. Integrated contributions from parts of current are identical for any distribution, but interferences may differ vastly. Analysis of option 1 is expected to give very poor insight on interferences, and options 2-4 can give only limited information. Option 5 is expected to give the best way to explore models in that regard. Yet, it still does not explore the whole structure of multidimensional phase-space, contrary to methods of Ref. [4].

## 9 TAUOLA CLEO, TAUOLA CLEO isospin intricate, CLEO publ.

Beside functional form of currents, numerical parameters affect shapes of distributions. Among them, mainly masses, widths, and couplings of the intermediate resonances differ. That is why, we collect all constants to the last detail, taking into account variants in the implementations. The set of parameters<sup>18</sup> is extracted from the **TAUOLA** code, to make sure that they were used in **TAUOLA CLEO** and **TAUOLA CLEO isospin intricate** currents. These currents rely on analysis of data using **option 5**, but further cross-checks using **option 6**, were also mentioned in CLEO publications. Published experimental data for  $\tau \rightarrow \pi^0\pi^0\pi^-\nu_\tau$  were used by the collaboration. Predictions for  $\tau \rightarrow \pi^-\pi^-\pi^+\nu_\tau$  were documented only in conference contributions [10, 11]. It is not the theoreticians or MC authors right to decide whether predictions for the  $\pi^-\pi^-\pi^+$  channel should be obtained from the  $\pi^0\pi^0\pi^-$  case at the level of distribution or taking into account isospin rotation of intermediate states. Actual choice must rely on analysis of systematic errors. Our default current **TAUOLA CLEO** implies that one considers contributions from intermediate states:  $f_0$ ,  $f_2$ ,  $\sigma$  as effective ways to improve distributions. We use then distribution level isospin symmetry to get predictions for  $\pi^-\pi^-\pi^+$  from  $\pi^0\pi^0\pi^-$ ; we use the same current for the two cases. Second variant, **TAUOLA isospin intricate**, was also prepared by the collaboration but was not published. We have nonetheless distributed it together with all versions of **TAUOLA**, but not made available for direct **TAUOLA** use<sup>19</sup>. To activate it, modification of code was always necessary. Let us stress that the numerical difference between the two options is comparable/smaller than the differences to other parameterizations presented in later sections. We believe also that the choice lies within the systematic uncertainties. This would of course have changed with CLEO publication or with the future publications of other collaborations. For further discussion and numerical comparison of different current options see the following subsections and Sections 11, 12.

---

<sup>18</sup>Note: we present here only those parameters that are different as only those can introduce any discrepancies between **CLEO publ.** and **TAUOLA CLEO**. The complete list of parameters is given in Section 11.

<sup>19</sup>There are other options of hadronic currents distributed, but never made available for general use as well. The aim was to stimulate future work or for archivization. That was for example the case of  $\pi^-\pi^-\pi^+\pi^0$  current used for background modeling in Delphi analysis of Ref. [32] and  $(K\pi\pi)^-$  currents of OPAL [33]. Alternative ALEPH parameterization of hadronic currents was documented in Refs. [8, 9].

The model described in Ref. [6] and the implementation used in **TAUOLA** differ only by parameters stored in Table 1. One should stress that Ref. [6] is for the  $\pi^0\pi^0\pi^-$  mode, whereas **TAUOLA CLEO** use the same current for the  $\pi^-\pi^-\pi^+$  mode as well.

TAUOLA CLEO	CLEO of Ref. [6]
$M_\rho = \text{MRO} = 0.7743 \text{ GeV}$	$M_\rho = \text{MRO} = 0.774 \text{ GeV}$
$\Gamma_\rho = \text{GRO} = 0.1491 \text{ GeV}$	$\Gamma_\rho = \text{GRO} = 0.149 \text{ GeV}$
$M_\tau = 1.777 \text{ GeV}$	not mentioned in the paper
$M_{a_1} = 1.275 \text{ GeV}$	$M_{a_1} = 1.331 \text{ GeV}$
$\Gamma_{a_1} = 0.700 \text{ GeV}$	$\Gamma_{a_1} = 0.814 \text{ GeV}$

Table 1: Parameters differing in **TAUOLA** and Ref. [6]. These differences in parameters are the reason of differences visible in Figure 1.

Analytic form of **TAUOLA CLEO isospin intricate** current for  $\tau \rightarrow \pi^-\pi^-\pi^+\nu_\tau$  can be understood as a simple consequence of isospin symmetry applied to the  $\tau \rightarrow \pi^0\pi^0\pi^-\nu_\tau$  case. But we must make sure if the hadronic current to be transformed by isospin rotation is sufficiently established, see discussion in section 14.1.

One could wonder, if it is not better to drop the terms of  $\sigma$ ,  $f_0$  and  $f_2$  from the current parameterization, so currents for both channels would have the same functional form. Indeed, that was often the case. For example, parametrizations **TAUOLA BaBar** and **TAUOLA RChL 2012** introduced later, used identical currents for  $\pi^-\pi^-\pi^+$  and  $\pi^0\pi^0\pi^-$ . In **TAUOLA CLEO** the same current for both channels was used disregarding the fact that it was seemingly introducing  $\sigma$  of a charge  $\pm 2$ . In fact, it was simply assumed that  $\sigma$  was just a feature of the current parametrization and *not* a real physical state. This is supported by the observation that on Dalitz plot from Fig. 3 of Ref. [10] there seems to be a resonance-like structure in  $s_3$ , the invariant mass of the  $\pi^-\pi^-$  pair. In corresponding plot, Fig. 5 of Ref. [6] for  $\pi^0\pi^0\pi^-$  case, the same structure can be seen in  $\pi^0\pi^0$ . It is most likely originating in part from interferences, but it can be parameterized as a resonance<sup>20</sup>. Let us now look into numerical differences between basic variants.

## 9.1 Numerical differences of **TAUOLA CLEO** and **CLEO publ.**

The MC sample presented in [6] is not available now, therefore we can only try to recreate results. To do so, we need to identify all differences in initializations. It appears, that only a few parameters differ, see Table 1. Resulting difference is small but clear on, see Fig. 1. Note, that these two variants used fixed values for masses and widths of resonances (while RChL and BaBar models fitted them). We can only speculate it is either due to stability<sup>21</sup> of fit procedure or simply the belief that use of results from other (non  $\tau$ ) measurements is better. Apart from extreme kinematic regions, the largest differences can be observed in  $\pi^-\pi^-\pi^+$  distribution.

<sup>20</sup> See also Section 14.2 where we discuss some possible origins of unexpected structures.

<sup>21</sup> Overpopulation of parameters may affect stability. If that was not the case, we may suspect lack of computing power, as additional parameters increase CPU time needed for fit to converge substantially.

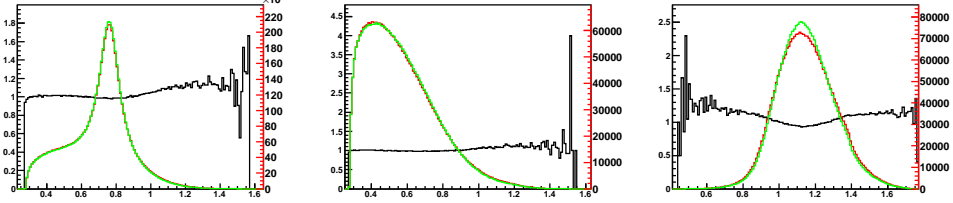


Figure 1: Invariant mass, GeV units, of (from the left)  $\pi^-\pi^+$ ,  $\pi^-\pi^-$ ,  $\pi^-\pi^-\pi^+$  in **TAUOLA CLEO** with numerical constants shifted to values of Ref. [6] (red) and **TAUOLA CLEO** with default parameterization (green). For black line which represent ratio of red plot to green one, left hand side scale should be used. Right hand side scale represent number of events per bins of 10 MeV.

We can also investigate differences in terms of three-dimensional plots. Fig. 14 presents Dalitz plots obtained from **TAUOLA CLEO**. As we do not have data nor MC generated sample from the CLEO collaboration, only human eye comparison is possible with their published results. Mentioned Fig. 14 of our paper should coincide<sup>22</sup> with Fig. 5 of. Ref. [6]. No convincing differences can be seen.

## 9.2 Numerical differences of TAUOLA CLEO and TAUOLA CLEO isospin intricate

These two currents have the same values of parameters but differ by functional form of hadronic current for  $\tau \rightarrow \pi^-\pi^-\pi^+\nu_\tau$ . **TAUOLA CLEO** is represented by equations (5), (6), while **TAUOLA CLEO isospin intricate** by eqs. (8), (9). The differences are large, see Fig. 2, judging with today standards for measurements, but not larger than of relatively recent parameterizations **TAUOLA RChL** and **TAUOLA RChl 2012** shown later in Fig. 6. In fact they are at the 10% level, that is at the level of the theoretical uncertainty for use of isospin symmetry [1].

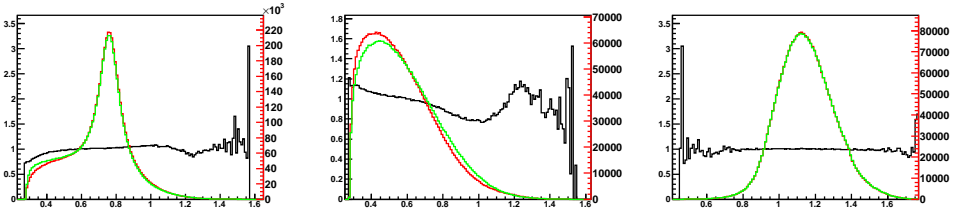


Figure 2: Invariant mass of (from the left)  $\pi^-\pi^+$ ,  $\pi^-\pi^-$ ,  $\pi^-\pi^-\pi^+$  in **TAUOLA CLEO** (red) and **TAUOLA CLEO isospin intricate** (green). For details of histograms definition see caption of Fig. 1.

<sup>22</sup> Note, results of Ref. [6] measurements are for the  $\pi^0\pi^0\pi^-$  mode, but the same functional form of hadronic current is used for the  $\pi^-\pi^-\pi^+$  in **TAUOLA CLEO**, that is why such comparison is valid.

## 10 Further variants of currents used by CLEO

Currents described in this paper are not the only ones developed by experimental collaborations. We would like to hint why certain solutions were used and documented in publications while others seem to be forgotten.

We should start the discussion with **CLEO publ.** This current is fully described in Ref. [6]. But the very same publication mentions a couple of other different variants, stating for some of them even better agreement with the data. So why is that any of those did not become main model of the collaboration?

First, we should mention variant of model where  $\sigma$  mass and width were fit parameters. Best agreement<sup>23</sup> with the data was obtained with  $M_\sigma = 555$  MeV and  $\Gamma_\sigma = 540$  MeV (page 22 of Ref. [6]). Such fit caused shift in all couplings not exceeding 20%. We may again only speculate that it was believed that it is better to use theoretically predicted or experimentally well established values. Fitting of sigma mass and width was probably performed in order to check how seriously this resonance should be treated. Result: different values than used for nominal model ( $M_\sigma = 860$  MeV and  $\Gamma_\sigma = 880$  MeV), was most likely not very encouraging.

Secondly, there is mentioned in Ref. [6] a study on pseudo-scalar contribution from  $\pi(1300)$ . It also improved the fit result, but with available data its existence could not be established with unquestioned significance. The very same reasoning was present in study of  $a'_1$  contribution, which also was not included in nominal model.

PhD thesis [12] presents similar study of pseudo-scalar  $\pi(1300)$  in  $\tau \rightarrow \pi^-\pi^-\pi^+\nu_\tau$  decay. Different ways of inclusion of scalar current were tested there. Similarly agreement with the data got better, but was not considered significant enough. In this study hadronic current used for non-scalar part was the same as **TAUOLA CLEO isospin intricate**. It suggests again, that at some point the current without pseudo-scalar contribution was used by the collaboration.

Another thing under consideration by CLEO was the resonance radius. Their study showed small importance. Therefore, it was set to 0 in order to simplify the model. Keeping things as simple as possible seem to be important for many choices of collaborations.

The BaBar collaboration had all CLEO currents available, yet decided to use simpler currents. Apart from simplicity, one can suspect another reason behind such a choice. The BaBar collaboration use commonly one-dimensional histograms in analysis even in our times [34]. Inclusion of any resonances other than  $\rho$  and  $\rho'$  is not to be easily exploited without three-dimensional distributions. On Fig. 3 one can see, that differences are not very compelling. They are mostly below 10%. Comparison of data and theoretical model on scatter-grams like Fig. 20 can show more clearly importance of other resonances, but it was never performed. On the last figure, ratio of Dalitz plots coming from BaBar model and CLEO model is shown. While ratio of invariant mass distributions was mostly between 0.9-1.1, ratio in some areas of Dalitz plots escapes 0.5-2 range.

---

<sup>23</sup>Negative doubled logarithmic likelihood was 43 units below that of nominal fit.

## 11 Comparison of TAUOLA CLEO, TAUOLA CLEO isospin intricate and TAUOLA BaBar

In this section comparison of CLEO and BaBar model used in TAUOLA is shown. Parameters are divided into three groups depending on the way they are introduced into the code and how they were used. Tab. 2 presents those defined globally, outside form factors. Table 3 presents those introduced inside hadronic current only. Parameters in this table were kept constant during the fitting procedure of CLEO, but were fitted for BaBar modeling. Table 4 stores parameters fitted to the data. They are also defined inside hadronic current. Note, that some parameters can be different for diverse parts of code, for example mass of  $\rho$  resonance. This may be misleadingly worrisome, but it should not be considered as an error. Parameters used outside hadronic form factors affect optimization of efficiency of phase-space generators, that is essentially speed of generation only, or are well established constants like  $m_\pi$ . Their variation does *not* affect output distributions, or variations are simply unphysical.

TAUOLA CLEO	TAUOLA BaBar
	$m_{\pi^0} = \text{AMPIZ} = 0.134996 \text{ GeV}$ $m_\pi = \text{AMPI} = 0.139570 \text{ GeV}$ $M_\rho = \text{AMRO} = 0.775 \text{ GeV}$ (used in GFUN) $M_{a_1} = \text{AMA1} = 1.251 \text{ GeV}$ $\Gamma_{a_1} = \text{GAMA1} = 0.599 \text{ GeV}$ $\beta = \text{BET} = 0$

Table 2: Parameters defined outside form factors (stored in INIMAS).

The **TAUOLA CLEO** code is essentially as described in Ref. [6] and named 'nominal fit'. It differs by some numerical constants only, see Table 1. The CLEO collaboration did not fit masses and widths of resonances but only coupling constants  $\beta_i$ . Such choice was driven by theoretical assumptions and measurements of masses elsewhere. This may be the best solution when we lack good enough measurements of state used in model. Let us recall, Section 10, how insensitive the model can be to the  $\sigma$  meson properties.

### 11.1 Numerical comparison of TAUOLA CLEO and TAUOLA BaBar

Here, we present numerical comparison of **TAUOLA CLEO** and **TAUOLA BaBar**. On Fig. 3, distributions of invariant masses of  $\pi^-\pi^+$ ,  $\pi^-\pi^-$ ,  $\pi^-\pi^-\pi^+$  are shown. Looking at the plots one notice that except the lack of some resonances mentioned earlier, also lack of  $K^*K$  threshold in BaBar model is visible in distribution of  $\pi^-\pi^-\pi^+$  mass (and even more visible on ratio plot) in 1.4 GeV region. Moreover, different  $a_1$  mass plays a role. In addition, on Fig. 20 of Appendix C, ratio of Dalitz plots is shown. Lack of  $f_0$ ,  $f_2$ ,  $\sigma$  resonances in model used by BaBar can be also seen there. Differences are higher than for

TAUOLA CLEO	TAUOLA BaBar
$M_\rho = \text{MRO} = 0.7743 \text{ GeV}$	$M_\rho = \text{ROM} = 0.773 \text{ GeV}$ (used in Breit-Wigner)
$\Gamma_\rho = \text{GRO} = 0.1491 \text{ GeV}$	$\Gamma_\rho = \text{ROG} = 0.145 \text{ GeV}$
$M_{\rho'} = \text{MRP} = 1.370 \text{ GeV}$	$M_{\rho'} = \text{ROM1} = 1.370 \text{ GeV}$
$\Gamma_{\rho'} = \text{GRP} = 0.386 \text{ GeV}$	$\Gamma_{\rho'} = \text{ROG1} = 0.510 \text{ GeV}$
$M_{f_2} = \text{MF2} = 1.275 \text{ GeV}$	$\beta_1 = \text{BETA1} = -0.145$
$\Gamma_{f_2} = \text{GF2} = 0.185 \text{ GeV}$	
$M_{f_0} = \text{MF0} = 1.186 \text{ GeV}$	
$\Gamma_{f_0} = \text{GF0} = 0.350 \text{ GeV}$	
$M_\sigma = \text{MSG} = 0.860 \text{ GeV}$	
$\Gamma_\sigma = \text{GSG} = 0.880 \text{ GeV}$	
$m_{\pi_0} = \text{MPIZ} = 0.134976 \text{ GeV}$	
$m_\pi = \text{MPIC} = 0.139570 \text{ GeV}$	
$m_{K^0} = \text{MK} = 0.496 \text{ GeV}$	
$M_{K^*} = \text{MKST} = 0.894 \text{ GeV}$	
$M_{a_1} = \text{AMA1} = 1.275 \text{ GeV}$	
$\Gamma_{a_1} = \text{GAMA1} = 0.700 \text{ GeV}$	
$\beta_1 = \text{BT1} = 1$	

Table 3: Parameters used in definition of hadronic currents in TAUOLA; both variants of CLEO parameterization and BaBar parameterization. This table stores parameters that were not fitted by the CLEO collaboration, but were taken from PDG tables or theoretical predictions. Corresponding BaBar parameters are stored here for completeness.

comparison of **TAUOLA CLEO isospin intricate** and **TAUOLA CLEO**, see Fig. 1. Invariant mass of  $\pi^- \pi^+$  system exhibits biggest difference in terms of ratio.

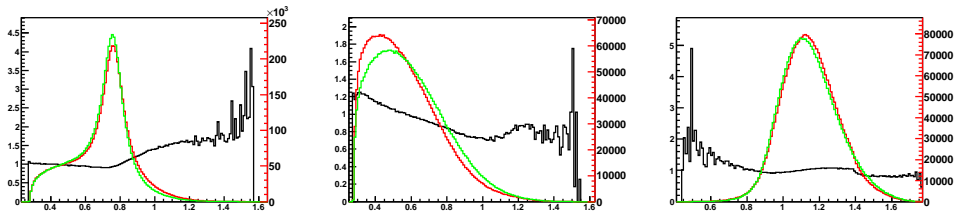


Figure 3: Invariant mass of (from the left)  $\pi^- \pi^+$ ,  $\pi^- \pi^-$ ,  $\pi^- \pi^- \pi^+$  in **TAUOLA CLEO** (red) and **TAUOLA BaBar** (green). For details of histograms definition see caption of Fig. 1.

$\beta_2 = \text{BT2} = 0.12e^{i0.99\pi}$
$\beta_3 = \text{BT3} = 0.37e^{-i0.15\pi}$
$\beta_4 = \text{BT4} = 0.87e^{i0.53\pi}$
$\beta_5 = \text{BT5} = 0.71e^{i0.56\pi}$
$\beta_6 = \text{BT6} = 2.10e^{i0.23\pi}$
$\beta_7 = \text{BT7} = 0.77e^{-i0.54\pi}$
$C_{3\pi} = \text{C3PI} = 0.2384^2$
$C_{K^*} = \text{CKST} = 4.7621^2 C_{3\pi}$

Table 4: Parameters used in definition of CLEO hadronic current in TAUOLA obtained by the CLEO collaboration from fit to the data.

## 11.2 Numerical comparison of TAUOLA CLEO isospin intricate and TAUOLA BaBar

For completeness we provide comparison of **TAUOLA CLEO isospin intricate** and **TAUOLA BaBar**. Results are very similar to previous comparison and can be seen on Fig. 4. We do not discuss those results as no new aspects appear. Largest difference is present in  $\pi^-\pi^+$  invariant mass spectrum.

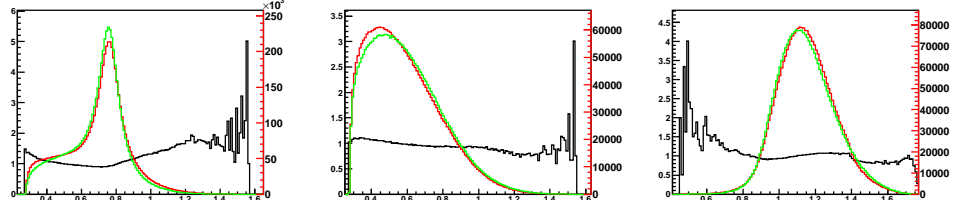


Figure 4: Invariant mass of (from the left)  $\pi^-\pi^+$ ,  $\pi^-\pi^-$ ,  $\pi^-\pi^-\pi^+$  in **TAUOLA CLEO isospin intricate** (red) and **TAUOLA BaBar** (green). For details of histograms definition see caption of Fig. 1.

## 12 Comparison of TAUOLA CLEO and TAUOLA RChL

In this section, numerical comparison of CLEO and RChL model used in TAUOLA is shown. We will not recall analytic form of RChL current. Full description of **TAUOLA RChL 2012** current is given in Ref. [20] (see also [13]), and for **TAUOLA RChL** in Ref. [14]. CLEO and RChL models differ a lot in a way of construction and also in parameters, but one may easily guess what affects the spectra in a way as seen on Fig. 5. Most importantly, inclusion and parameters of  $\sigma$  resonance are different. The  $\sigma$  of lower mass and width than in the CLEO model, affects mainly low mass region of  $M(\pi^-\pi^+)$  in RChL, while in CLEO model it affects the whole spectra. Second, clearly visible difference appears in  $\pi^-\pi^-\pi^+$  invariant mass distribution. It comes from different modeling of  $a_1$ . CLEO

translated theoretical modeling into polynomial of eq. (7). RChL keeps direct model coded, but parameters of  $K^*$  meson were not fitted, as the  $\pi^-\pi^-\pi^+$  channel should not be very sensitive to them. Reasonable modification of those parameters would require simultaneous fit of the  $KK\pi$  channel. Such fit could possibly reduce difference in area of the  $K^*K$  threshold mentioned in previous section.

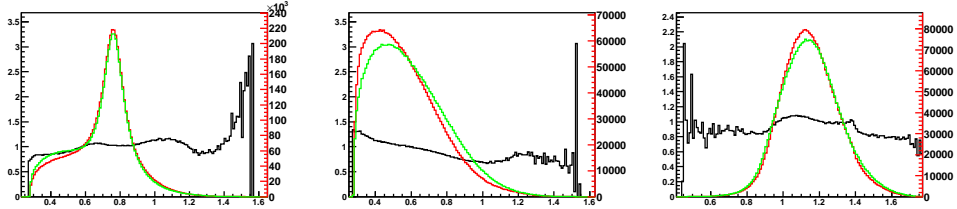


Figure 5: Invariant mass of (from the left)  $\pi^-\pi^+$ ,  $\pi^-\pi^-$ ,  $\pi^-\pi^-\pi^+$  in **TAUOLA CLEO** (red) and **TAUOLA RChL** (green). For details of histograms definition see caption of Fig. 1.

In Fig. 21 of appendix C, we can find three-dimensional ratio of RChL to CLEO model results. On that plot, we can see areas where difference between the models exceeds factor of 2. This is much bigger difference than seen on one-dimensional distributions. As CLEO model was fitted to three-dimensional distribution it is a very worrisome observation from the RChL perspective. It may hint that even though one-dimensional BaBar data distributions are described well [14], underlying physics model may be imperfect. Actual judgment should not be completed without comparison with experimental distributions of higher dimensionality.

## 12.1 Comparison of TAUOLA RChL 2012 and TAUOLA RChL

For completeness, we present comparison of first version of RChL model and a new one. Because of the comparison with the data, especially inability to obtain satisfactory agreement in  $\pi^-\pi^+$  invariant mass, when all invariant mass distributions were fitted simultaneously **TAUOLA RChL 2012** was modified. Those two models differ mainly by inclusion of  $\sigma$  resonance in the **TAUOLA RChL** version. Other differences are model parameters and minor correction for Coulomb interaction. Resulting differences in distributions can be seen on Fig. 6.

At this point we must emphasize that those two versions of RChL model were fitted to different data-sets. Invariant mass of  $\pi^-\pi^-$  system became available for fits only after development of **TAUOLA RChL 2012**. This model was fitted to invariant masses of  $\pi^-\pi^+$ ,  $\pi^-\pi^-\pi^+$  systems only, while **TAUOLA RChL** to invariant masses of  $\pi^-\pi^+$ ,  $\pi^-\pi^-$ ,  $\pi^-\pi^-\pi^+$ . It was not the only difference. Also binning of histograms changed. New version was fitted to histograms of 10MeV bin width<sup>24</sup>. Distributions used in fit of **TAUOLA RChL 2012** had bin width of 20MeV.

---

<sup>24</sup> This kind of binning is used in all one-dimensional plots of our paper.

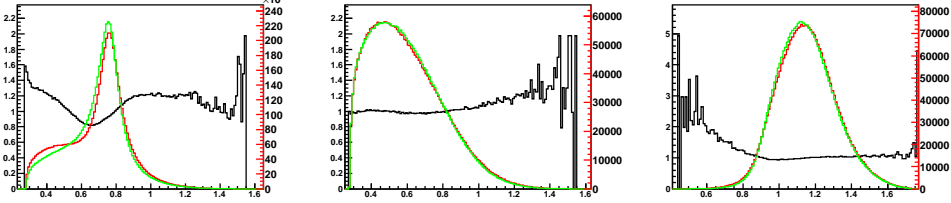


Figure 6: Invariant mass of (from the left)  $\pi^-\pi^+$ ,  $\pi^-\pi^-$ ,  $\pi^-\pi^-\pi^+$  in **TAUOLA RChL** (red) and **TAUOLA RChL 2012** (green). For details of histograms definition see caption of Fig. 1.

## 13 Numerical effects of interferences within currents

So far, we have concentrated on presentation of different currents used for Monte Carlo simulations of  $\tau$  decays. We have looked into their analytical form as well as the numerical values of the parameters fixed by confrontations with experimental data. Comparisons obtained from different parameterizations were reported as well. In the present Section let us look into numerical consequences of some features of the currents. We will concentrate on interferences between distinct parts of the current, which can be separated, with the help of isospin transformation.

Final states of long-living scalars with given multiplicity and charge combination, can be formed through intermediate resonances used in description of hadronic current. One can not think of them as sum of non coherent contributions. Interferences represent important aspect of hadronic current which should be understood and controlled. Even if used for fits experimental distributions are correctly reproduced, unnatural response to modifications of individual contributions to the current and interference can hint for modeling flaws.

In principle, addition of a new resonance to the hadronic current should result in negative interference below the peak and positive above<sup>25</sup>. There is no clear prediction on how strong such resonance should interfere. In case of a narrow intermediate resonance we expect such interference to cancel out in contributions to total rates or relatively inclusive distributions. Especially in case of wide resonances, we may model a process with something that is not of proper dynamical nature but still describes data quite well, simply by accident.

In this section, we will investigate RChL and CLEO modeling of the three-pion channels. We concentrate on interference of part depending on isoscalars<sup>26</sup> with the remaining part of the current. These two parts of hadronic current transform differently under isospin rotation. In principle it is also a test on how justified (or not) is isospin rotation from  $\pi^0\pi^0\pi^-$  to  $\pi^-\pi^-\pi^+$  currents.

Let us look at the contribution to the rate. For  $\pi^0\pi^0\pi^-$ , the  $\rho$  part, the  $\sigma, f_2, f_0$  part

<sup>25</sup> That is true in case when resonances come in with the same sign. In our case signs are opposite.

<sup>26</sup> Contribution only from  $\sigma$  in RChL, while for CLEO from  $\sigma, f_2, f_0$ .

and their interference contribution are respectively<sup>27</sup> 75.1%, 4.4% and 20.5%. Usage of **TAUOLA CLEO isospin intricate** current for  $\pi^-\pi^-\pi^+$  gives 74%, 5.8% and 20.2%. Interference looks slightly different for fully differential distributions. Then, it is 22.6% in **TAUOLA CLEO**, and 20.7% for **TAUOLA CLEO isospin intricate** case, when method as explained in Section 8 is used. For the three-dimensional scatter-grams of the CLEO collaboration style, see Appendix C for details, the interference is respectively 22.3% and 20.6%. This demonstrates nearly perfect sensitivity of such a method.

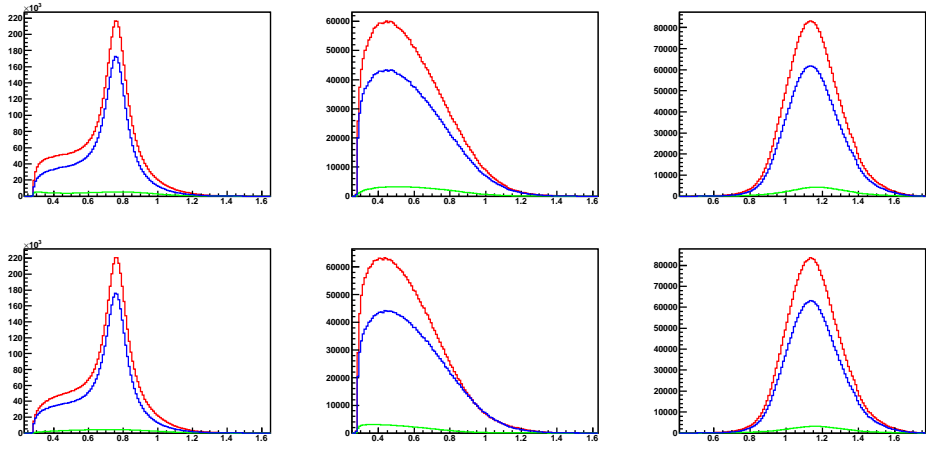


Figure 7: Invariant mass of (from the left)  $\pi^-\pi^+$ ,  $\pi^-\pi^-$ ,  $\pi^-\pi^-\pi^+$  using **TAUOLA CLEO isospin intricate** (top) and **TAUOLA CLEO** (bottom). Green plot represents contribution from isoscalars ( $\sigma, f_2, f_0$ ) and blue from remaining part. Red plot represents the whole current. Blue and green plots would sum up to red one, in the absence of interference. Percentages of the three contributions are given in Table 5.

Current	Absolute width	1D distributions	3D distributions	Absolute width differential
$\pi^0\pi^0\pi^-$ CLEO	75.1% 4.4% 20.5%	75.1% 4.4% 20.8%	75.1% 4.4% 22.4%	75.1% 4.4% 22.7%
$\pi^-\pi^-\pi^+$ CLEO	75.3% 4.3% 20.4%	75.3% 4.3% 20.7%	75.3% 4.3% 22.3%	75.3% 4.3% 22.6%
$\pi^-\pi^-\pi^+$ CLEO isospin intricate	74% 5.8% 20.2%	74% 5.8% 20.2%	74% 5.8% 20.6%	74% 5.8% 20.7%
$\pi^-\pi^-\pi^+$ RChL	97.5% 6.5% 4%	97.5% 6.5% 11%	97.5% 6.5% 18.2%	97.5% 6.5% 18.5%
$\pi^0\pi^0\pi^-$ RChL	94% 1.3% 4.7%	94% 1.3% 7.4%	94% 1.3% 9.5%	94% 1.3% 10%

Table 5: Comparison of contributions from the isoscalars from the remaining part of the current and from interference, depending on a way of investigation. In each cell, first number is from the spin one intermediate states, second is from isoscalars and the third one is interference. For 1-D (one-dimensional) distributions interference effect of the histogram with largest effect is taken. In the case of "Absolute width differential", average of (module of) interference over all events is shown.

In Table 5 we collect such results also for other versions of the currents. One must remember that the interference visible in histograms is somewhat dependent on binning. We do not have the same binning as the CLEO collaboration; they had less bins per energy

<sup>27</sup> When the same current is used for  $\pi^-\pi^-\pi^+$  corresponding contributions are 75.3%, 4.3% and 20.4%.

unit in every distributions. Therefore, while they probably could have seen the same behavior, the interference observed was most likely smaller. Interference is an important numerical property of the distributions which can not be ignored while making the choices for phenomenological approach<sup>28</sup>.

Having discussed CLEO modeling let us investigate the same problem in RChL model. On Fig. 8, one can compare contributions from different parts of current on one-dimensional distributions. We can see that plot follows theoretical expectation on how interference should look. Also, there is much less interference than for CLEO models, see Table 5. Moreover, size of interference for the one-prong and three-prong channels is not as similar as in CLEO modeling. While both CLEO models have almost the same level of interference in both channels, RChL has twice more in the three-prong channel. Also, size of  $\sigma$  contribution differ a lot between the one- and the three-prong channels, while it is close to the same in both CLEO modelings. Another property worth noting is limited sensitivity of RChL model to interference when only one-dimensional distributions are used. It means that the most recent fit of this model does not fully control<sup>29</sup> influence of  $\sigma$  and fit to three-dimensional distributions is strongly desired.

As both models aim at describing the same decay channels we should be concerned that interplay of internal parts of the current is quite different. It proves that we do not have good understanding of physics behind it, especially what exactly is the  $\sigma$  state, in at least one of the two approaches. Both models find it important [6] [14] to include  $\sigma$ , but its description is far from consistent<sup>30</sup>.

## 14 Interplay of experimental and theoretical input

In the process of creating a model for hadronic current to be used in MC there are two aspects. Theoreticians provide model for hadronic currents and experimentalists use it and fit parameters. Usually, theoreticians concentrate on consistency of formulation and prefer to avoid ad hoc phenomenological corrections. Very often, model building is disconnected from data analysis. On the other hand, experimentalists would like to have model perfectly

<sup>28</sup> Later, in particular in Section 14.2 we discuss how resonances are deformed and even can produce artificial peaks. Therefore, resonances are not always needed to emulate peaks present in experimental distribution. Also, because shapes of resulting modifications to distributions are distinct with respect to, e.g., Gaussian peaks of resonance parameterizations, we can be concerned about choice between **TAUOLA CLEO** and **TAUOLA CLEO isospin intricate**. This especially, as dominant contribution of isoscalars is a result of interference. Confrontation with the experimental data should be used to resolve this matter.

<sup>29</sup> The reason why interference effect is better visible in one-dimensional distributions in case of CLEO model than in RChL is technically quite simple. In the first case the mass of the  $\sigma$  is larger so the region of phase-space above the peak is restricted, no cancellation occurs. Nonetheless it is important to realize such features while evaluating suitability of experimental input for the model fit. It should not be assumed that the conclusion will remain the same for all range of the fit parameters.

<sup>30</sup> We may speculate that in part, this difficulty in control contribution from isoscalars was a reason behind introduced later much simpler current in BaBar Monte Carlo simulations. Note, that in Ref. [14] parameters of  $\sigma$  contributions were featuring errors from the fit larger than for other resonances. We will return to this point in Section 14.

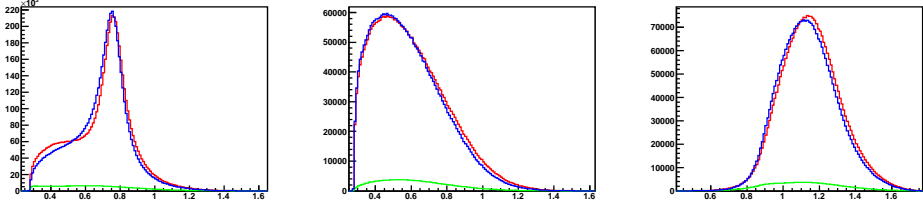


Figure 8: Invariant mass of (from the left)  $\pi^-\pi^+$ ,  $\pi^-\pi^-$ ,  $\pi^-\pi^-\pi^+$  using **TAUOLA RChL** current. Green plot represents contribution from isoscalars and blue one from remaining part. Red plot represents whole current. Blue and green plots should sum up to red one in the absence of interference. One can see negative interference for RChL model whereas it was almost everywhere positive for **TAUOLA CLEO isospin intricate**, see Fig. 7. and Table 5.

describing the data. At the same time, they must have control over any possible sources of experimental errors. Therefore, they may prefer to sacrifice some model assumptions for the sake of simplicity and more straightforward systematics analysis<sup>31</sup>. As experiment controls data sample it is experimentalists to give "stamp of approval" for the hadronic current. Such thing was done for  $\pi^0\pi^0\pi^-$  current of CLEO modeling, but is lacking for  $\pi^-\pi^-\pi^+$  case. Only conference contributions describe some modelings of this channel. In case of the CLEO modeling we may only speculate if there were some unresolved problems with this channel or it was simply lack of the manpower that stopped the collaboration publication from appearing. In the following subsections we will discuss some aspects of model-building that can play a role.

### 14.1 Ambiguities of experimental inputs

Isospin symmetry between  $\tau$  decay channels, can be restricted to a relation of final states only. As a consequence, for intermediate states, such a choice could be understood as including contribution of e.g.,  $\sigma \rightarrow \pi^-\pi^-$  for the channel  $\tau \rightarrow \nu_\tau\pi^-\pi^-\pi^+$ . This of course would mean an error. However, as  $\sigma$  was not well established (and very broad) resonance at the time of the CLEO work, this may not be unreasonable. Back then,  $f_0(400-1200)$  [35] with width ranging from 400-1000 MeV was expected. Later on, in years 2002-2012  $f_0(600)$  was expected [36]. Recently, in 2012 it was shifted to  $f_0(500)$  [37], thanks to numerous calculations, e.g., [38, 39] claiming both mass and width close to 500 MeV. In current measurements this resonance remain extremely wide, while the CLEO collaboration used even wider (880 MeV) and more massive (860 MeV)  $\sigma$ , as of Ref. [40].

That is why, from the experimentalist point of view, one can think of this amplitude contribution as a heuristic modification for the current, of not much quantum number meaning<sup>32</sup>. Such interpretation may hold, unless it is excluded by comparisons with exper-

<sup>31</sup> In particular that there are no strongly correlated parameters in the fits.

<sup>32</sup> In Ref. [6] we read: *The form factors as defined in Eqn. A2 (Equation A2 of Ref. [6] corresponds*

imental data. In the meantime, such an option in the Monte Carlo, can be helpful to study if the contribution is indeed the  $\sigma$ . Alternatively, it is possible to think that broad  $\sigma$  is just a pretext to correct current of  $a_1$ ,  $\rho$  intermediate states, thus may be identical for one- and three-prong  $\tau$  decay modes. Similarly one can think of  $f_0$ . The  $f_2$  is not as broad, but even in this case contributions to  $s_1$ ,  $s_2$  spectra are not clearly localized in the phase-space. We should also mention that both  $f_2$  and  $f_0$  have limited phase-space for decay, therefore their Breit-Wigner distributions are strongly deformed. On top of that, in Section 13 we have shown that isoscalars in the models we have presented, do not contribute as separate resonances to the decay. They contribute positive interference over almost whole spectra. That is why, such imposed isospin symmetry understood as use of the same current for the  $\pi^-\pi^-\pi^+$  and the  $\pi^0\pi^0\pi^-$  decay channels of  $\tau$  can be justified. Let us recall that isospin symmetry may be broken and of limited predictive power starting from 5-10% precision level (Ref. [1] Section 5.11). Also, there is very small contribution to the currents from isospin violating decays<sup>33</sup>.

## 14.2 Further concerns for model-data confrontation

Let us look into details of the **TAUOLA CLEO isospin intricate** current, and the decay channel  $\tau \rightarrow \pi^-\pi^-\pi^+\nu_\tau$ . The contribution from isoscalars may be missed from the distribution of  $\pi^-\pi^+$  invariant mass spectrum: no clean features are seen, Fig. 9 green line. If we artificially increase by a factor of 10 isoscalars amplitude, they dominate the shape of  $\pi^-\pi^+$  invariant mass spectrum, see red line, but clear peaks are still absent. Position of the peaks is shifted with respect to the masses used in the propagator<sup>34</sup> of hadronic current. One can see, blue line, that two peaks emerge clearly if widths of isoscalars are reduced by a factor of 10 as well. Looking at all three lines, one realizes that appearing low energy peak/deformation present in **TAUOLA CLEO isospin intricate** (in other modelings as well) is in a big part indirect. There are two possible combinations of  $\pi^-\pi^+$  and both are put into the histogram. Lower peak-like bump comes from small phase-space available for  $\pi^-$  when system of other  $\pi^-$  and  $\pi^+$  is produced with high invariant mass. That forces low invariant mass bump for the  $\pi^-\pi^+$  system, even though those two pions do not originate from a common intermediate resonance.

Resonances at the end of the phase-space represent challenging part of the description. As we could see from Fig. 9, their shapes are substantially deformed from the ones of Breit-Wigners. The other effect is also possible. In Ref. [43] it was demonstrated how

---

*to our eq. (1)) do not have simple correspondence with those that can be associated with specific resonant contributions to the hadronic current,* which seem to support our statement.

<sup>33</sup> In the  $\tau \rightarrow 3\pi\nu_\tau$  decay mode isospin violating signals are expected [41]. There are two decays that can feed  $3\pi$  spectrum. For the three-prong channel it is  $\tau \rightarrow \omega\pi^-\nu_\tau$  with subsequent  $\omega \rightarrow \pi^-\pi^+$  decay. The one-prong channel can be fed by the decay  $\tau \rightarrow \eta\pi^0\pi^-\nu_\tau$  (due to  $\eta - \pi^0$  mixing). Those decays are estimated to give small contribution to the total rate at the level of 0.4% and  $10^{-3}\%$ , respectively. Studies of  $\tau \rightarrow \eta\pi^0\pi^-\nu_\tau$  case were also done within RChL scheme [42].

<sup>34</sup>See formulae (6), (5), and Tables 2, 3, 4 for the definition of  $\rho$ ,  $\sigma$ ,  $f_2$ , and  $f_0$  propagators as used by the CLEO collaboration.

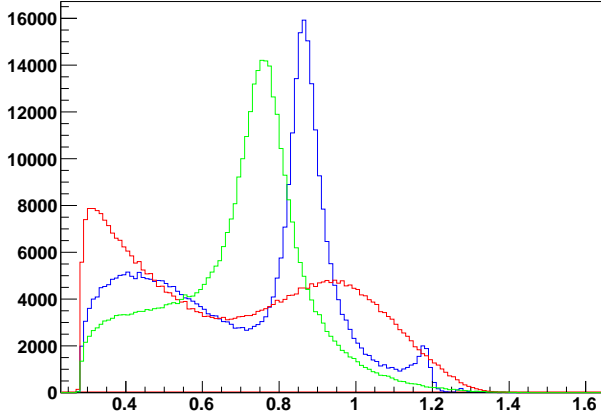


Figure 9: Invariant mass of  $\pi^-\pi^+$  system in  $\tau \rightarrow \pi^-\pi^-\pi^+$  decay using **TAUOLA CLEO isospin intricate** (green), current with multiplied 10 times amplitude from isoscalars (red) and also with width of isoscalars reduced 10 times (blue).

deformations due to resonances acting as phase-space constraints, may result even in artificial resonance-like peaks. This observation is another reason why one may be hesitant to exploit isospin symmetries of currents in an uncritical way.

Another concern is the size of contribution due to interference. It may be much larger than the effect of extra resonances alone. At the same time, it is not fully explored by inclusive distributions. See Table 5; for RChL, interference effect is much larger for the three-dimensional histograms than for the one-dimensional ones. For the CLEO case, the difference was rather minor. One has to remember of such effects, while introducing new resonances into the currents. It must be carefully studied if they affect shapes of the distributions in a controlled way.

Finally, if numerical effects are small and weakly depend on model parameters, Monte Carlo methods may not be best suited for the studies. Especially if systematic errors are to be taken into account [44]. If available, semi-analytical methods are better. Therefore, we have prepared special arrangement which is briefly presented in Appendix A.

## 15 Summary

In this paper, we have investigated several variants of parameterizations of hadronic currents used in Monte Carlo programs for simulations of the  $\tau$  lepton decays. As a reference for comparisons we have used **TAUOLA CLEO** parameterization, because of its well established status; it is supported by the collaboration publication. The first investigated variant was **TAUOLA CLEO isospin intricate**, as prepared for TAUOLA but not commonly used. This parameterization is documented by conference contribution only. We have evaluated the numerical size of the differences, which were found to be of the order

of systematic errors expected from the use of isospin symmetry alone. We have looked for the origin of numerical differences. We studied both analytic forms of the distributions as well as dependence on numerical constants.

Later, we have presented comparisons with further parameterizations, in particular the variants of **TAUOLA RChL 2012**, **TAUOLA RChL** and **TAUOLA BaBar**. All distributions were obtained with the help of Monte Carlo generations. We have prepared semi-analytical distributions to calculate such results as well. This is a necessary step toward fitting with the help of multidimensional distributions, using variants of model independent methods presented in Ref. [4], but adopted to the case, when  $\tau$  leptons are relativistic (that is when  $\nu_\tau$  momentum cannot be reconstructed easily).

We have discussed limitations and constraints on use of models and symmetries like isospin symmetry resulting from insufficiently differential distributions of experimental data. We have pointed to large numerical consequences of interferences. We have also pointed out problems related to phase-space constraints for decay products of broad resonances.

We should accept that predictions of the RChL models may agree with the data with precision not worse than  $\frac{1}{N_C}$  that is about 30% (in respect to total rate) only. Indeed, all of the presented parameterizations pass such condition and agree with each other at that level as well. Precision of the experimental data is at least one order of magnitude better. That is why, one has to concentrate the effort on arrangements for convenient comparisons of the data with model predictions. It is important that models are prepared in sufficiently flexible way (the necessary future adaptations can be introduced fast and correlations of parameters are understood) before the fits to experimental data are performed. Also experimental distributions need to be investigated, if they are detailed enough to constrain the underlying physics.

We have discussed consequences of limited dimensionality of distributions used in data representations for results of fits. We could see in Ref. [14], that the model of  $\tau \rightarrow 3\pi\nu_\tau$  decay modes, prepared only a year earlier [20] and fitted to two, one-dimensional, mass histograms, turned out to predict results for the invariant mas of  $\pi^-\pi^-$  pair rather poorly. It had to be updated. We are expecting this to repeat once three-dimensional experimental histograms are addressed. There is a factor of two discrepancy between RChL models and CLEO models results for some bins of the three-dimensional distributions (which were used by CLEO also as input to their fits). One-dimensional histograms may thus not be enough as experimental input for precise parameterization of hadronic currents. The three-dimensional ones of the type as used by CLEO [6] may be sufficient for  $\tau \rightarrow 3\pi\nu_\tau$ . However, this conjecture may need to be checked before serious work on the  $\tau$  decay channels into 3 scalars with kaons, like that of Refs. [45, 46] is completed. Then, full complexity of hadronic currents is expected, and analysis similar to the one of Ref. [4] may be indispensable. Nonetheless, attempts to construct currents on the basis of fits to one-dimensional (three-dimensional CLEO style) distributions are of interest. It can demonstrate predictive power of models such as RChL beyond  $\frac{1}{N_C}$  precision level. On a practical side, once differences and options are understood in context of one-dimensional distributions, we are better prepared to fit the high precision data of today.

If operators like those in Ref. [4] are needed, then they have to be adopted for conditions of  $\tau$  leptons produced relativistically (making reconstruction of  $\nu_\tau$  momentum non trivial). Our paper documents also a step of work into such direction, see also web page [47].

Even though the purpose of our paper is to review available options for hadronic currents used in simulation of  $\tau$  decays into  $3\pi$ , some speculations, why such choices were introduced in the past, were unavoidable. This is by far incomplete aspect of this work, and may be even misleading at some points. There is little documentation on internal discussions of experimental groups behind actual choice of analytical form of current parameterizations used in data analysis and publications. Often complicated and sometimes unfinished activities, where questions of great importance on systematic errors for multidimensional distributions were risen, could not be referred.

In general, we think experiments should be responsible for fits approving models quality. We hope our paper will contribute to discussion how relations between model developers, experimental physicists and people working on Monte Carlo and fitting programs should look.

## Acknowledgments

We are indebted to co-authors of our publications and experimental partners as well. We would like to thank: Simon Eidelman, Swagato Banerjee, Pablo Roig, Marcin Chrzaszcz, Tomasz Przedziński for discussions and for reading the manuscript.

## References

- [1] S. Actis *et al.*, *Eur. Phys. J.* **C66** (2010) 585–686, 0912.0749.
- [2] S. Jadach, J. H. Kühn, and Z. Was, *Comput.Phys.Commun.* **64** (1990) 275–299.
- [3] S. Jadach, Z. Was, R. Decker, and J. H. Kühn, *Comput.Phys.Commun.* **76** (1993) 361–380.
- [4] J. Kühn and E. Mirkes, *Zeitschrift fur Physik C Particles and Fields* **56** (1992), no. 4 661–671.
- [5] O. Shekhovtsova, 1506.08390.
- [6] CLEO Collaboration Collaboration, D. Asner *et al.*, *Phys.Rev.* **D61** (2000) 012002, [hep-ex/9902022](#).
- [7] G. Ecker, J. Gasser, H. Leutwyler, A. Pich, and E. de Rafael, *Phys. Lett.* **B223** (1989) 425.
- [8] P. Golonka, E. Richter-Was, and Z. Was, [hep-ph/0009302](#).
- [9] P. Golonka, B. Kersevan, T. Pierzchala, E. Richter-Was, Z. Was, *et al.*, *Comput.Phys.Commun.* **174** (2006) 818–835, [hep-ph/0312240](#).
- [10] CLEO Collaboration Collaboration, E. I. Shibata, *eConf* **C0209101** (2002) TU05, [hep-ex/0210039](#).

- [11] M. Schmidtler, *Nucl. Phys. Proc. Suppl.* **76** (1999) 271–282.
- [12] J. W. Hinson, *Axial vector and pseudoscalar hadronic structure in tau decays to three charged pions and a tau neutrino with implications on light quark masses*. PhD thesis, Purdue University, 2001.
- [13] D. G. Dumm, P. Roig, A. Pich, and J. Portolés, *Phys. Lett.* **B685** (2010) 158–164, 0911.4436.
- [14] I. Nugent, T. Przedziński, P. Roig, O. Shekhovtsova, and Z. Was, *Phys. Rev.* **D88** (2013), no. 9 093012, 1310.1053.
- [15] T. Sjöstrand, S. Ask, J. R. Christiansen, R. Corke, N. Desai, *et al.*, 1410.3012.
- [16] G. J. Gounaris and J. J. Sakurai, *Phys. Rev. Lett.* **21** (1968) 244–247.
- [17] Particle Data Group Collaboration, K. A. Olive *et al.*, *Chin. Phys.* **C38** (2014) 090001.
- [18] A. Rouge, [hep-ph/0303212](#).
- [19] N. Davidson, P. Golonka, T. Przedziński, and Z. Was, *Comput. Phys. Commun.* **182** (2011) 779–789, 0812.3215.
- [20] O. Shekhovtsova, T. Przedziński, P. Roig, and Z. Was, *Phys. Rev.* **D86** (2012) 113008, 1203.3955.
- [21] P. Roig, I. M. Nugent, T. Przedziński, O. Shekhovtsova, and Z. Was, *AIP Conf. Proc.* **1492** (2012) 57–61, 1208.4513.
- [22] J. H. Kühn and A. Santamaría, *Z. Phys.* **C48** (1990) 445–452.
- [23] S. Weinberg, *Physica* **A96** (1979) 327.
- [24] J. Gasser and H. Leutwyler, *Annals Phys.* **158** (1984) 142.
- [25] G. Colangelo, M. Finkemeier, and R. Urech, *Phys. Rev.* **D54** (1996) 4403–4418, [hep-ph/9604279](#).
- [26] G. 't Hooft, *Nucl. Phys.* **B72** (1974) 461.
- [27] E. Witten, *Nucl. Phys.* **B160** (1979) 57.
- [28] A. Bondar, S. Eidelman, A. Milstein, T. Pierzchala, N. Root, *et al.*, *Comput. Phys. Commun.* **146** (2002) 139–153, [hep-ph/0201149](#).
- [29] CMD-2 Collaboration, R. R. Akhmetshin *et al.*, *Phys. Lett.* **B466** (1999) 392–402, [hep-ex/9904024](#).
- [30] A. E. Bondar, S. I. Eidelman, A. I. Milstein, and N. I. Root, *Phys. Lett.* **B466** (1999) 403–407, [hep-ph/9907283](#).
- [31] J. H. Kühn and Z. Was, *Acta Phys. Polon.* **B39** (2008) 147–158, [hep-ph/0602162](#).
- [32] DELPHI Collaboration, P. Abreu *et al.*, *Phys. Lett.* **B426** (1998) 411–427.
- [33] OPAL Collaboration, G. Abbiendi *et al.*, *Eur. Phys. J.* **C13** (2000) 197–212, [hep-ex/9908013](#).

- [34] I. M. Nugent, SLAC-R-936, Ph.D. Thesis.
- [35] Particle Data Group Collaboration, C. Caso *et al.*, *Eur.Phys.J.* **C3** (1998) 1–794.
- [36] Particle Data Group Collaboration, K. Hagiwara *et al.*, *Phys.Rev.* **D66** (2002) 010001.
- [37] Particle Data Group Collaboration, J. Beringer *et al.*, *Phys.Rev.* **D86** (2012) 010001.
- [38] R. García-Martin, R. Kaminski, J. Peláez, and J. Ruiz de Elvira, *Phys.Rev.Lett.* **107** (2011) 072001, 1107.1635.
- [39] I. Caprini, G. Colangelo, and H. Leutwyler, *Phys. Rev. Lett.* **96** (2006) 132001, hep-ph/0512364.
- [40] N. A. Tornqvist, *Z.Phys.* **C68** (1995) 647–660, hep-ph/9504372.
- [41] E. Mirkes and R. Urech, *Eur.Phys.J.* **C1** (1998) 201–209, hep-ph/9702382.
- [42] D. G. Dumm and P. Roig, *Phys. Rev.* **D86** (2012) 076009, 1208.1212.
- [43] T. Ishikawa, Y. Kurihara, M. Skrzypek, and Z. Was, *Eur.Phys.J.* **C4** (1998) 75–84, hep-ph/9702249.
- [44] T. Przedziński, P. Roig, O. Shekhovtsova, Z. Was, and J. Zaremba, *Computer Science J.* **16** (2015) 17–38.
- [45] O. Shekhovtsova, *Nucl. Part. Phys. Proc.* **260** (2015) 52–55, 1411.3526.
- [46] D. G. Dumm, P. Roig, A. Pich, and J. Portoles, *Phys. Rev.* **D81** (2010) 034031, 0911.2640.
- [47] J. Zaremba, <http://annapurna.ifj.edu.pl/~jzaremba/klocki/fit-program.html>.
- [48] I. Antcheva *et al.*, *Computer Physics Communications* **180** (2009), no. 12 2499 – 2512, 40 YEARS OF CPC: A celebratory issue focused on quality software for high performance, grid and novel computing architectures.

## A Analytical distributions

From the reference [14] documenting RChL current and its fit to the experimental data it became obvious that having semi-analytical distributions available, simplifies and speeds up the fitting procedure. As a part of this work we have prepared a program to calculate distributions from given hadronic current by integrating the structure function  $W_A$  (as defined in Ref. [4]) within limits of a chosen bin. Program uses `IntegralMultiple` function of `ROOT` [48] libraries allowing acquisition of both one-dimensional and Dalitz distributions. We have checked the code to give proper results for **TAUOLA CLEO**, **TAUOLA CLEO isospin intricate**, **TAUOLA BaBar**, and **TAUOLA RChL**. Program offers easy way for re-fit of these models to the data of a form of three-dimensional distributions like in CLEO publication. Also, it is much easier, than if MC method is used, to perform analysis of statistical and systematical errors with the semi-analytical results free of statistical errors themselves. See Ref. [14] for details.

`IntegralMultiple` routine of `ROOT` library has several input parameters. In particular, minimum and maximum number of function evaluation requested for each bin. Those parameters affect precision and time of integration, therefore one has to find a balance between the two. We have found that integration has some stability problems if too low number of requested points is chosen. Taking into account time, precision, and stability of integration we choose minimum 5000 points and maximum 50 000 points per bin. With such setup it takes 6 sec (of CPU time on a typical PC processor) for **TAUOLA CLEO** and 16 sec for **TAUOLA RChL** to get one-dimensional distributions and respectively, 47 and 120 sec to get Dalitz plots with the same binning as presented in Appendix C. One has to add 2 sec for CLEO and 30 sec for RChL models for reinitialization whenever model parameters are changed. If higher precision is needed, doubling number of points per bin, requires 50% more time for three-dimensional plots while it does not noticeably affect calculation of one-dimensional distributions. We expect that CPU time for Dalitz plots calculation can still be optimized. Fit with Dalitz plots is more desired, it gives better test of investigated model and has simpler systematics calculation; each individual event enters only one bin in contrary to one-dimensional histograms where it enters each<sup>35</sup> of four histograms of invariant masses. In Ref. [44] optimization of fitting procedure for **TAUOLA RChL** in case of one-dimensional histograms is presented. We hope that with similar approach we could prepare framework allowing fast fitting to three-dimensional distributions for any theoretical model as well. Note, that current initialization of RChL is prepared for multiple channels of  $\tau$  decays, including not yet published ones with kaons [45, 46]. These, were not confronted with the data yet. For fitting to  $\pi^-\pi^-\pi^+\nu_\tau$  data, we can skip running routines needed for these other channels, to speed it up to the level which was used in Ref. [44]. We have not checked if `IntegralMultiple` will provide smooth distributions with model parameters variation. It is important for fitting algorithms that derivatives with respect to model parameters are continuous, as we have found while working for Ref. [14].

## B Comparison of TAUOLA CLEO and Pythia CLEO

In this appendix, we present comparison of alternative implementation of CLEO model for  $\tau \rightarrow \pi^-\pi^-\pi^+\nu_\tau$  as done in PYTHIA 8.201, with TAUOLA implementation. Thanks to comparison we can identify source of differences and estimate its impact on generated event samples.

By investigation of `Pythia` code, several differences in parameterization were found and stored in Table 6. Parameters not mentioned in that table are the same as for TAUOLA. Hadronic current of **Pythia CLEO** is of the same form as described in Section 4 for **TAUOLA CLEO isospin intricate**. Internal arrangements of the code are slightly different. Due to this; in structure of the code some constants are folded with others. Parameter  $\Gamma_{a_1}$  is one of such. It is not coded explicitly, but we can extract its value: 0.784468371 GeV.

---

<sup>35</sup> Each event enters histograms for invariant mass of  $\pi^-\pi^-$ ,  $\pi^-\pi^-\pi^+$  and twice for  $\pi^-\pi^+$  systems (as there are two possible pairs of  $\pi^-\pi^+$ ).

TAUOLA CLEO	Pythia CLEO
$M_\tau = 1.777 \text{ GeV}$	$M_\tau = 1.77699 \text{ GeV}$
$M_{a_1} = 1.275 \text{ GeV}$	$M_{a_1} = 1.331 \text{ GeV}$
$\Gamma_{a_1} = 0.700 \text{ GeV}$	is calculated, see section text
$\text{C3PI} = 0.2384^2$	$\text{C3PI} = 0.2384^2 / 1.0252088$
$\beta_3 = \text{BT3} = 0.37e^{-i0.15\pi}$	$\beta_3 = \text{BT3} = 3.7 \cdot 10^{-7}e^{-i0.15\pi}$
$\beta_4 = \text{BT4} = 0.87e^{i0.53\pi}$	$\beta_4 = \text{BT4} = 8.7 \cdot 10^{-7}e^{i0.53\pi}$
$\beta_5 = \text{BT5} = 0.71e^{i0.56\pi}$	$\beta_5 = \text{BT5} = 7.1 \cdot 10^{-7}e^{i0.56\pi}$

Table 6: Differences in numerical values of parameters used in **TAUOLA CLEO** and **Pythia CLEO**.

Figures 14 and 15 of Appendix C represent Dalitz plots from TAUOLA and Pythia, respectively. Fig. 17, shows ratio of Fig. 15 to Fig. 14. One-dimensional distributions of invariant mass of  $\pi^- \pi^+$ ,  $\pi^- \pi^-$ ,  $\pi^- \pi^- \pi^+$  for both generators can be seen on Fig. 10. There is systematic difference between generators. Disagreement may have appeared due to different form of hadronic current, or different numerical parameters. To test this, for both generators constants of Ref. [6] were taken. Agreement was not improved substantially, with the exception of invariant mass  $\pi^- \pi^- \pi^+$ , where influence of  $a_1$  mass and width turned out to be the main source of difference, as can be seen from Fig. 11. In general, agreement only to about 10 % can be concluded except some less populated bins at ends of  $\pi^- \pi^+$  mass spectra.

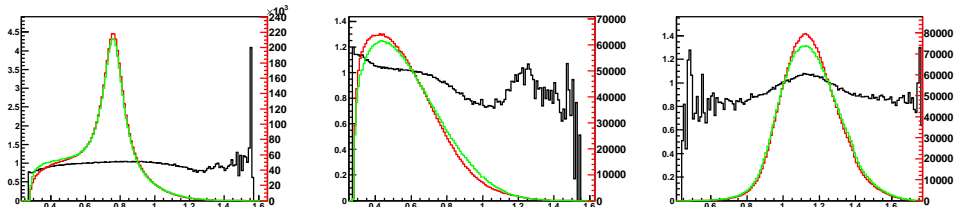


Figure 10: Invariant mass of  $\pi^- \pi^+$ ,  $\pi^- \pi^-$ ,  $\pi^- \pi^- \pi^+$  in **TAUOLA CLEO** (red) and **Pythia CLEO** (green). For details of histograms definition see caption of Fig. 1.

It suggests that functional form of hadronic current is of higher numerical importance, than model constants. To test this, we have used **TAUOLA CLEO isospin intricate** current while having the same parameters in both generators. As in previous test, constants were set that of [6]. Resulting distributions of invariant masses, as well as their ratios can be seen in Fig. 12: nearly perfect agreement can be concluded<sup>36</sup>.

To complete our investigation, comparison of **TAUOLA CLEO isospin intricate** and **Pythia CLEO**, with default initializations was performed. Generators use hadronic current of eqs. (8), (9), and only numerical constants differ as those collected in Table 6.

<sup>36</sup> This is also true for Dalitz plots, see Fig. 18.

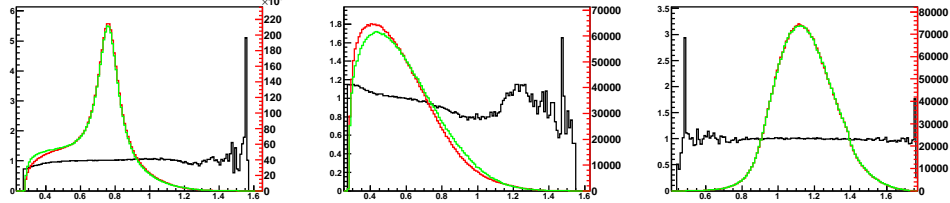


Figure 11: Invariant mass of  $\pi^- \pi^+$ ,  $\pi^- \pi^-$ ,  $\pi^- \pi^- \pi^+$  in **TAUOLA CLEO** (red) and **Pythia CLEO** (green), when the same parameters are enforced for both generators. For details of histograms definition see caption of Fig. 1.

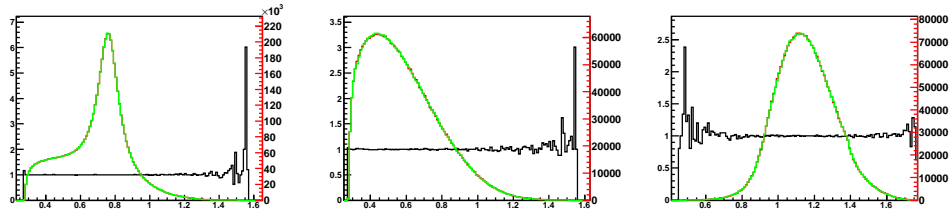


Figure 12: Invariant mass of  $\pi^- \pi^+$ ,  $\pi^- \pi^-$ ,  $\pi^- \pi^- \pi^+$  in **TAUOLA CLEO isospin intricate** (red) and **Pythia CLEO** (green), when the same parameters are enforced for both generators. For details of histograms definition see caption of Fig. 1.

Figure 13 shows resulting distributions of invariant masses and their ratios. One can see the biggest difference in invariant mass of  $\pi^- \pi^- \pi^+$  due to distinct  $a_1$  mass and width, which are of highest importance among all numerical constants.

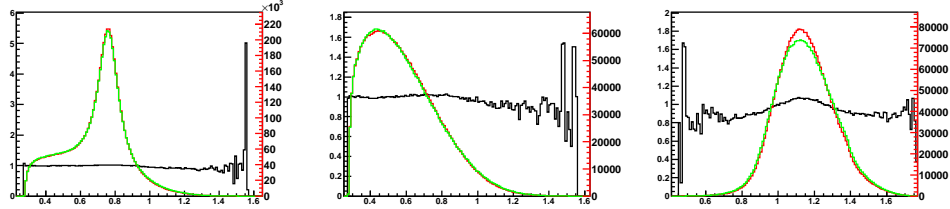


Figure 13: Invariant mass of  $\pi^- \pi^+$ ,  $\pi^- \pi^-$ ,  $\pi^- \pi^- \pi^+$  in **TAUOLA CLEO isospin intricate** (red) and **Pythia CLEO** (green). For details of histograms definition see caption of Fig. 1.

Further, technical checks were performed: the same numerical constants and the same but simplified hadronic current were installed in both generators. Those included:

- reducing hadronic current to  $F_1$  of eq. (5) only ( $F_2, F_3 = 0$ ).
- setting hadronic current to constant.
- reducing hadronic current to Breit-Wigner of  $a_1$  only.

In all these cases no discrepancies between results of **TAUOLA** and **Pythia** generators beyond statistical fluctuations were found. Samples of 3 million events were used.

All considered, differences in produced by **TAUOLA** and **Pythia** distributions for the  $\tau \rightarrow \pi^-\pi^-\pi^+\nu_\tau$  decay channel result only from parameters if the same variant of current is used in **TAUOLA**, otherwise generators perform identically. All differences are insignificant in comparison to parameterization uncertainties.

## C Cleo style results of 3-dimensional distribution

In this Appendix we collect 3 dimensional distributions for 3 scalar final states following definition used by CLEO [6]. For each figure, eight Dalitz plots in  $s_1$ ,  $s_2$  invariant masses are given for  $Q^2$  restricted, respectively to 0.36-0.81, 0.81-1.0, 1.0-1.21, 1.21-1.44, 1.44-1.69, 1.69-1.96, 1.96-2.25, 2.25-3.24 GeV $^2$  ranges.

Such representation does not constrain full differential nature of hadronic currents, but it was used in publication of experimental data of the most differential nature until now. It is an important reference point.

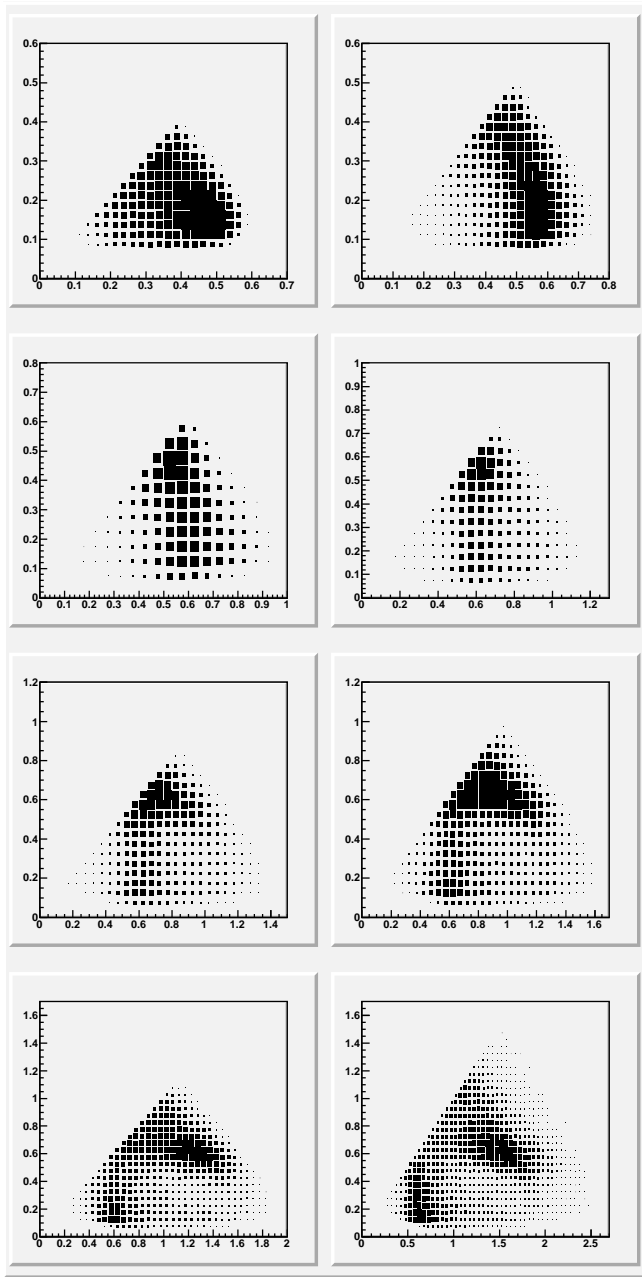


Figure 14: 8 Dalitz plots for slices in  $Q^2$ : 0.36-0.81, 0.81-1.0, 1.0-1.21, 1.21-1.44, 1.44-1.69, 1.69-1.96, 1.96-2.25, 2.25-3.24  $\text{GeV}^2$ . Each Dalitz plot is distribution for **TAUOLA CLEO** in  $s_1$ ,  $s_2$  variables ( $\text{GeV}^2$  units).  $s_1$  is taken to be the highest of the two possible values of  $M_{\pi^- \pi^+}^2$  in each event.

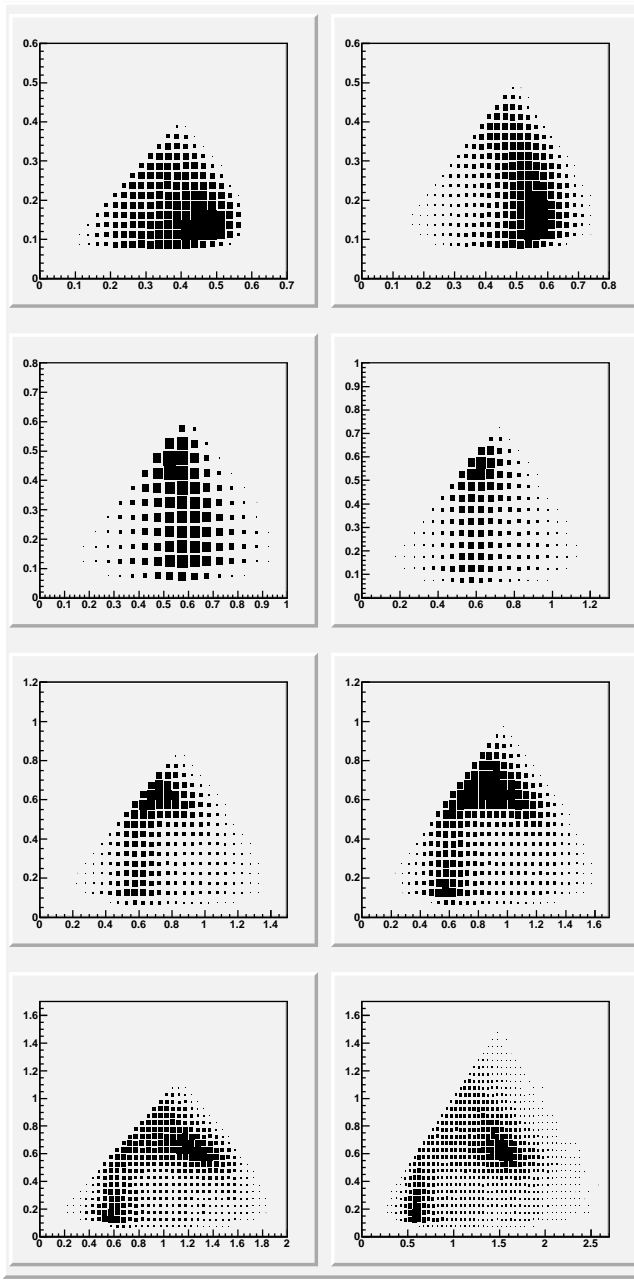


Figure 15: 8 Dalitz plots for slices in  $Q^2$ : 0.36-0.81, 0.81-1.0, 1.0-1.21, 1.21-1.44, 1.44-1.69, 1.69-1.96, 1.96-2.25, 2.25-3.24  $\text{GeV}^2$ . Each Dalitz plot is distribution for **Pythia CLEO** in  $s_1$ ,  $s_2$  variables ( $\text{GeV}^2$  units).  $s_1$  is taken to be the highest of the two possible values of  $M_{\pi^- \pi^+}^2$  in each event.

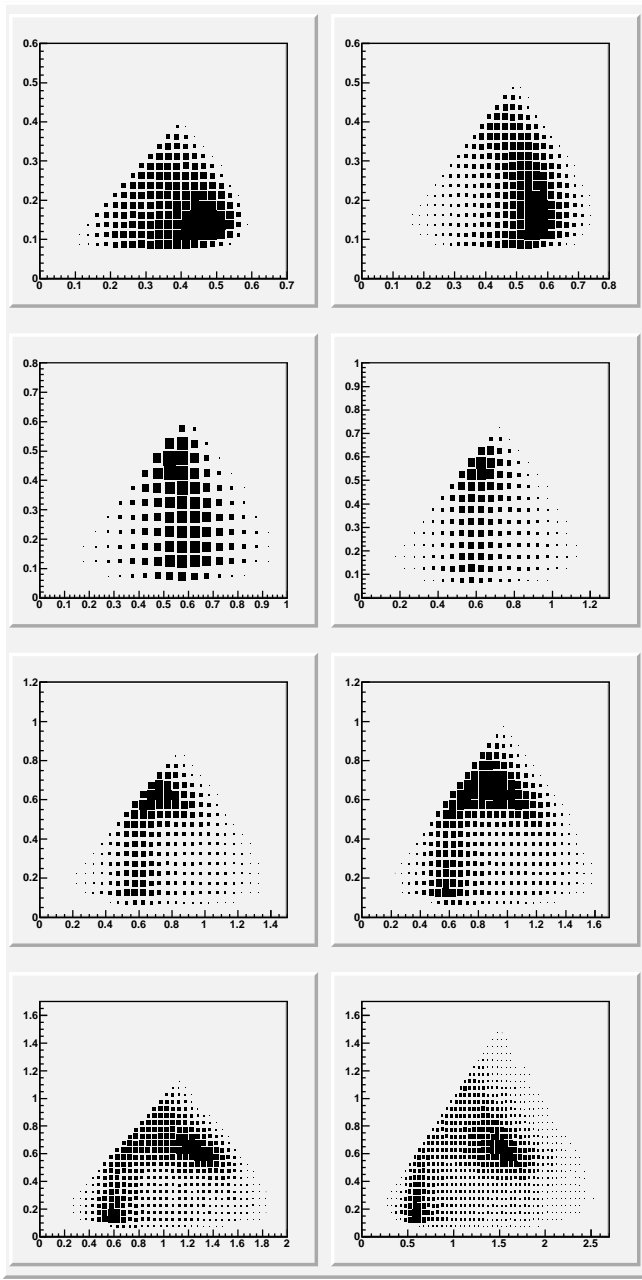


Figure 16: 8 Dalitz plots for slices in  $Q^2$ : 0.36-0.81, 0.81-1.0, 1.0-1.21, 1.21-1.44, 1.44-1.69, 1.69-1.96, 1.96-2.25, 2.25-3.24 GeV $^2$ . Each Dalitz plot is distribution for **TAUOLA CLEO isospin intricate** in  $s_1$ ,  $s_2$  variables (GeV $^2$  units).  $s_1$  is taken to be the highest of the two possible values of  $M_{\pi^-\pi^+}^2$  in each event.

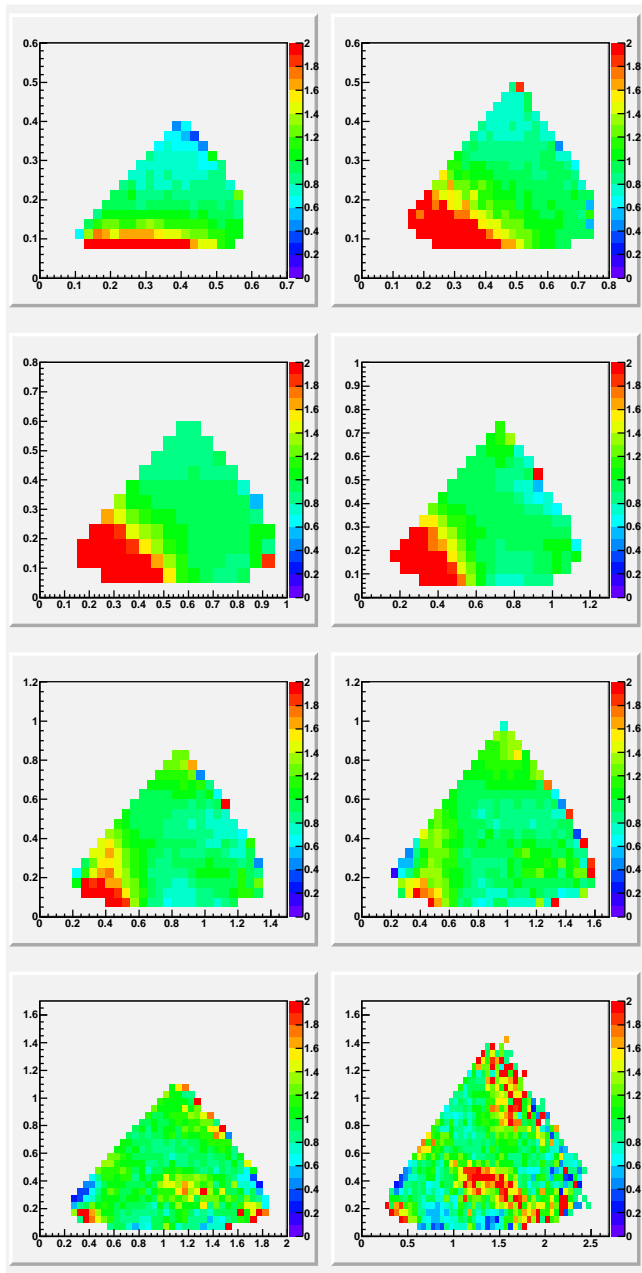


Figure 17: Ratios of **Pythia CLEO** to **TAUOLA CLEO** Dalitz plots (Figs. 15, 14).

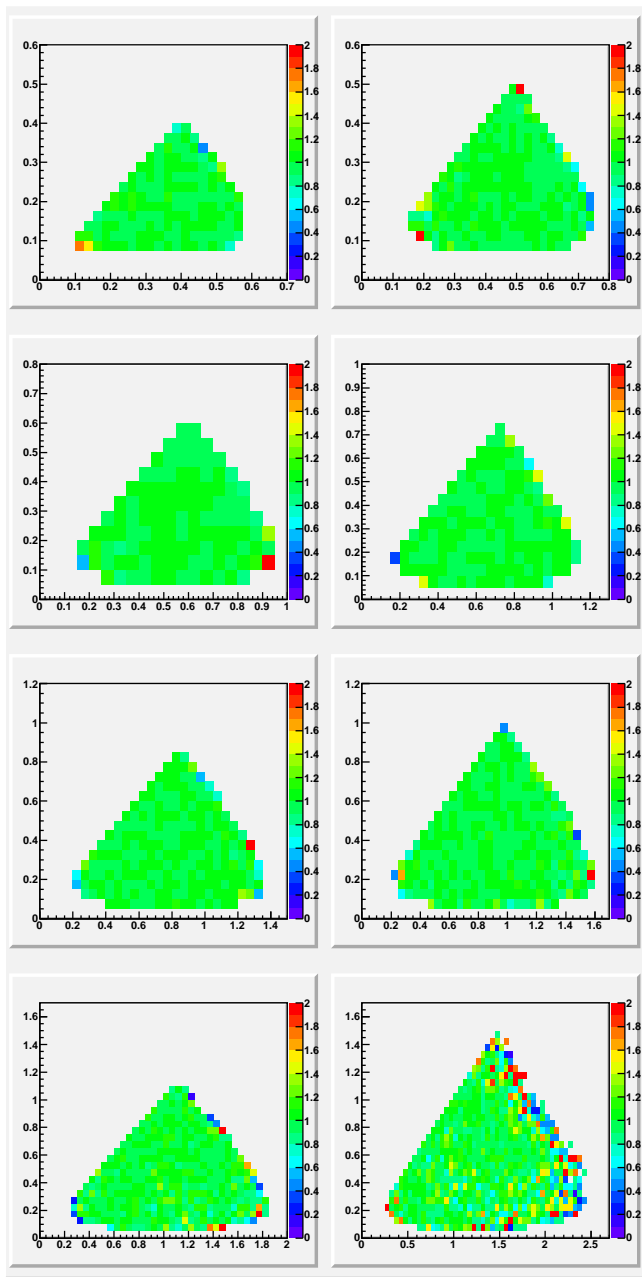


Figure 18: Ratios of **Pythia CLEO** to **TAUOLA CLEO** isospin intricate Dalitz plots (Figs. 15, 16).

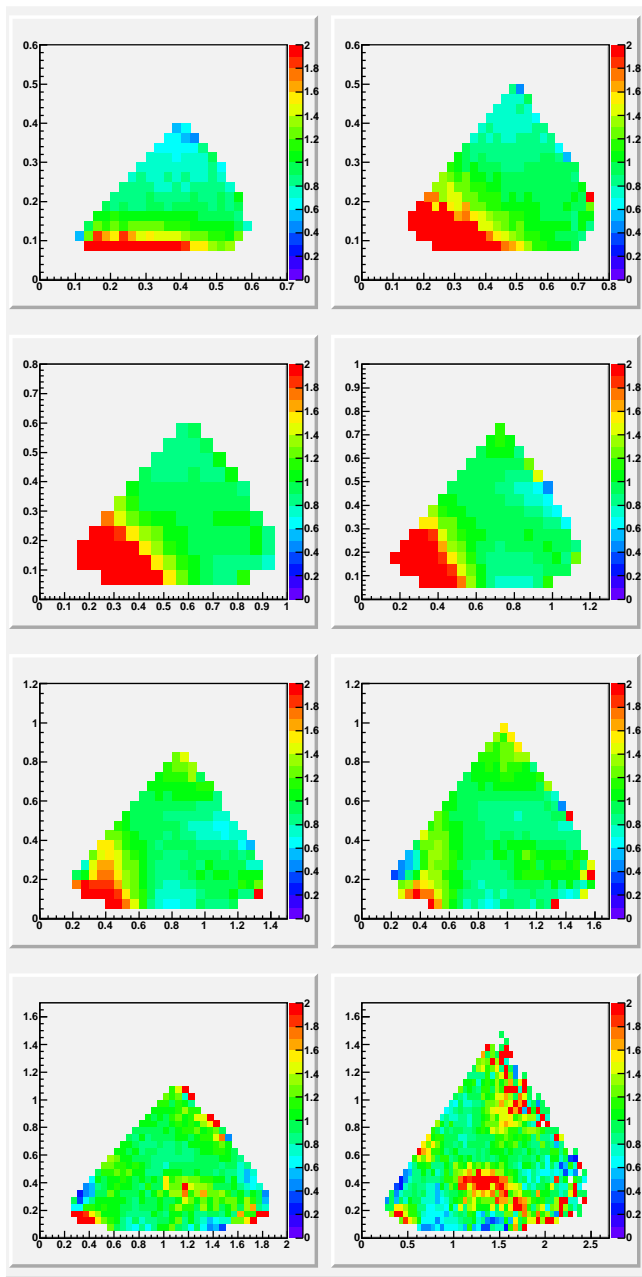


Figure 19: Ratios of **TAUOLA CLEO isospin intricate** to **TAUOLA CLEO Dalitz** plots (Figs. 16, 14).

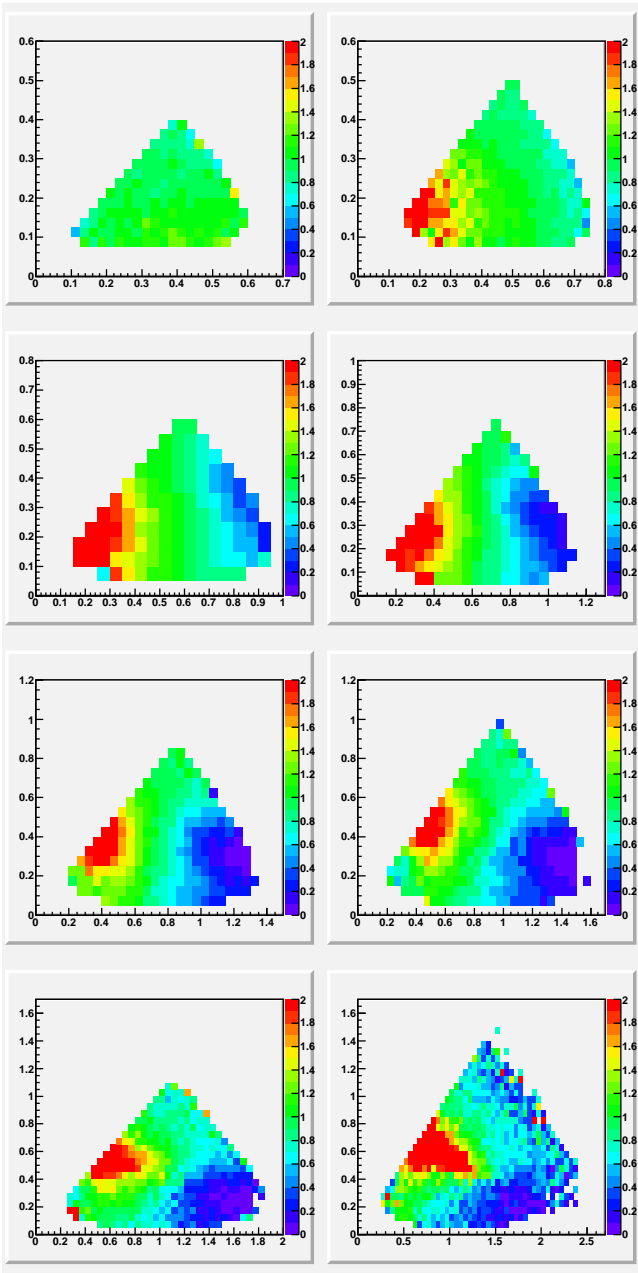


Figure 20: Ratios of **TAUOLA BaBar** to **TAUOLA CLEO** Dalitz plots in  $s_1$ ,  $s_2$  variables (GeV $^2$  units). Consecutive plots correspond to slices in  $Q^2$ : 0.36-0.81, 0.81-1.0, 1.0-1.21, 1.21-1.44, 1.44-1.69, 1.69-1.96, 1.96-2.25, 2.25-3.24 GeV $^2$ .

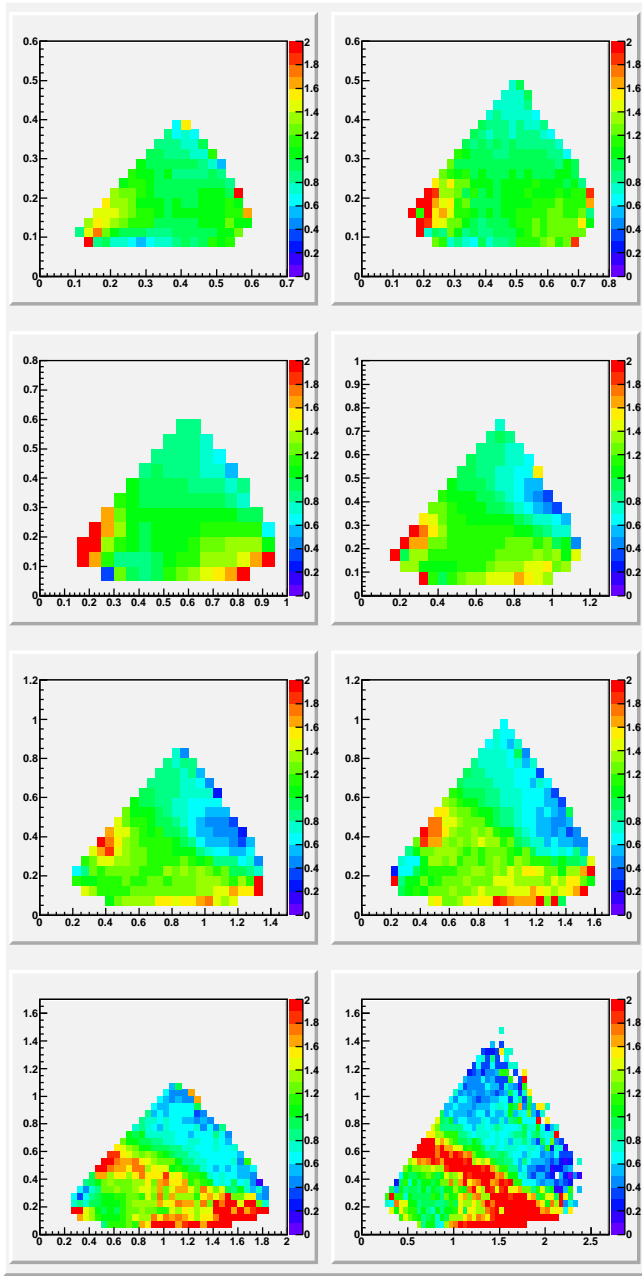


Figure 21: Ratios of **TAUOLA RChL** to **TAUOLA CLEO** Dalitz plots in  $s_1, s_2$  variables (GeV $^2$  units). Consecutive plots correspond to slices in  $Q^2$ : 0.36-0.81, 0.81-1.0, 1.0-1.21, 1.21-1.44, 1.44-1.69, 1.69-1.96, 1.96-2.25, 2.25-3.24 GeV $^2$ .